MAGNETIC ABRASIVE FINISHING OF NON-FERROMAGNETIC ROLLING ELEMENTS

By

MICHAEL J. FOX

Bachelor of Science

Oklahoma State University

Stillwater, Oklahoma

1992

Submitted to the Faculty of the
Graduate College of the
Oklahoma State University
in partial fulfillment of
the requirements for
the Degree of
MASTER OF SCIENCE
December, 1994

MAGNETIC ABRASIVE FINISHING OF
NON-FERROMAGNETIC ROLLING ELEMENTS

Thesis Approved:

R Komanduri
Thesis Adviser

Don A. Lucca

C E Price

R Komanduri for T. R. Thomas

Thomas C. Collins
Dean of the Graduate College

PREFACE

The purpose of this research is to develop a technique for finishing non-ferromagnetic structural materials, such as 303 stainless steel and hot pressed silicon nitride. The surface of these components must be both smooth, and free of defects such as micro-cracks, and also free from subsurface damage. To accomplish this task, a technology known as magnetic abrasive finishing (MAF) was applied to finish cylindrical non-magnetic materials.

Rational in magnetic abrasive finishing a magnetic field is provided to attract magnetic abrasive particles toward the workpiece, thus providing a pressure between the abrasive particles and the work. The workpiece is then rotated, which provides the relative motion between the workpiece and the abrasive particles. The magnetic poles which provide the magnetic field for the finishing process are usually vibrated in the workpiece's axial direction, which adds a second velocity to that which is provided by the rotary motion. The purpose of the axial vibration is to prevent the abrasive particles from cutting grooves around the workpiece and to generate a specific lay surface if desired. The overall abrasive particle path which results from the two velocity components, is "S" shaped, with the exact geometry depending on the relative magnitude of the two velocity components.

The pressure between the magnetic abrasives and the workpiece, in the case of a non-ferromagnetic workpiece, is dependent on the magnetic properties of the magnetic

abrasive powder, distribution of the magnetic field, and intensity of the magnetic field. The distribution of magnetic field is controlled by the shape of the magnetic poles, and the intensity may by varied by changing the current supplied to the coils of the electromagnet which supplies the magnetic field. In general, an increase in the supplied current to the electromagnetic coils, results in an increase in the finishing pressure. The current in this investigation is controlled by a microcomputer, which enables the field intensity to automatically vary as a function of time.

The workpiece material used in this investigation is 303 stainless steel rods. This particular material was chosen because stainless steel is used extensively for many applications where corrosion resistance is critical. Also these materials are difficult to machine and finish to high accuracies. The non-ferromagnetic property also enables it to be used for simulation of other non-ferromagnetic materials such as silicon nitride. The low cost of ground 303 stainless steel rods offers an inexpensive starting material for the present study.

Some of the variables which were identified include workpiece characteristics such as roundness, hardness, and roughness; process parameters such as workpiece rotational velocity, magnetic pole vibrational amplitude and frequency, magnetic field strength and distribution; and also magnetic abrasive properties such as material, structure and grain size. The information obtained and experience gained from experimentation with stainless steel workpieces aid in the determination of a starting point for finishing silicon nitride components.

The final objective of this investigation is to polish a silicon nitride rolling element

reaching a surface roughness below 10 nm Ra[1], which will demonstrate the viability of this process with respect to finishing advanced ceramics.

This investigation shows that MAF technology offers a low cost alternative to conventional lapping and grinding and reduces the cost of equipment from nearly $1,000,000 for an ultraprecision grinder, to on the order of a few thousand for adaption of MAF equipment to a conventional precision machine tool. It is also shown that this technology is capable of finishing silicon nitride to roughnesses on the order of a few nanometers in a matter of minutes, as opposed to the hours, days, or even weeks required for traditional methods of polishing such brittle materials.

[1]see Section 4.2 for definitions of quantitative parameters.

ACKNOWLEDGMENTS

I wish to thank Dr. R. Komanduri for introducing me to engineering research, and for providing me with this research opportunity. I would also like to thank him for his guidance and inspiration during the last two years.

I express my sincere appreciation for my other committee members Dr. D. Lucca, Dr. E. Misawa, Dr. R. Mohan, and Dr. C. E. Price for their time, guidance, and suggestions provided during this research.

The magnetic abrasive finishing apparatus was designed and built by Dr. T. Shinmura of Utsunomia University as part of a collaberative research with professor R. Komanduri of Oklahoma State University. The author has, however, integrated the computer with the apparatus as well as the motions of the Hardinge lathe on which this apparatus was mounted. The author acknowledges Dr. T. Shinmura's contributions to the present investigations.

Thanks are also due to H. Yamaguchi, K. Agrawal, M. Cole, M. Dock, D. Horinek, B. Sekher, and C. Parsons for their help taking data and building equipment, and to Dr. N. Umehara of Tohoku University, Japan, for his contributions to this project.

This project was funded in part by a contract (F33615-92-5933) from the ARPA Ceramic Bearing Program, and by a grant (DDM-9402895) from the National Science Foundation for the design and development of magnetic field assisted polishing equipment. I would like to thank Dr. W. Coblenz of ARPA, Dr. Karl R. Mecklenburg of WPAFB, and Dr. K. Srinivasan and Dr. B. M. Kramer of the National Science Foundation for their interest in this work.

TABLE OF CONTENTS

LIST OF FIGURES

LIST OF SYMBOLS AND NOMENCLATURE

A	Amplitude of vibration
d	Diameter of abrasive grain
D	Diameter of magnetic abrasive agglomerate, Diameter of workpiece
F	Force
H	Magnetic field strength
L	Length
MAF	Magnetic Abrasive Finishing
Ra	Roughness average
Ra_0	Initial roughness before finishing
Ra_f	Roughness after finishing
Rku	Kurtosis
Rq	RMS roughness
Rsk	Skewness
Rt	Peak to valley roughness
t	time
V	Volume
V_r	Velocity resulting from workpiece rotation
V_{vmax}	Maximum velocity resulting from pole vibration
x_n	Electronegativity of element n
x	Horizontal position
z	Deviation from mean height
θ	Half included angle of abrasive path
μ	Permeability

μ_0	Permeability of vacuum
τ	Time constant during finishing
ω	Frequency of vibration
Ω	Rotational speed of workpiece
X	Magnetic Susceptibility

Chapter I

Introduction

Magnetic abrasive finishing (MAF) is a finishing technique that uses magnetic force to induce pressure between ferro-magnetic abrasive particles and a workpiece. In this investigation a cylindrical workpiece is used. It is mounted in a chuck of a precision lathe and rotated, which results in a relative velocity between the abrasive and the workpiece. The combination of pressure and relative velocity facilitates in the finishing (polishing) action on the workpiece.

The MAF process is of technological value due to its ability to finish cylindrical parts with good surface finish, and high geometric accuracy. These cylinders may then be used for rolling elements for bearing applications. Ultra-precision grinding machines that are capable of producing comparable components are very expensive. However, MAF equipment is relatively simple compared to ultra-precision grinders, and may therefore offer high precision cylindrical finishes, at a fraction of the cost of ultra-precision grinding.

MAF was originally developed in the United States prior to world war II. This work was extended by Baron and his associates from the former USSR during the 1970's [Baron, 1986]. Mekedonski and his associates from Bulgaria also explored this field during the same period [Mekedonski, 1974]. Based on the Russian and Bulgarian work,

Japanese researchers, chiefly Takazawa, Shinmura, and Hitano, conducted extensive research in the 1980's [Takazawa et al., 1983]. They investigated the principles of operation and finishing characteristics of the MAF process on cylinders, and later extended inner surfaces of non-ferromagnetic tubes. Although magnetic abrasive finishing is capable of finishing non-ferromagnetic materials, the non-ferromagnetic properties of these materials lead to the difficulty in obtaining high magnetic field strengths. Low magnetic field strength results in low finishing pressures, which make finishing non-ferromagnetic materials difficult using this process. For this reason, research on finishing non-ferromagnetic materials has been quite limited.

1.1 Problem Statement

The purpose of this research is to investigate the MAF process when applied to non-ferromagnetic materials. Capabilities of the process, such as finishing pressure, are determined. Topics including the effect of magnetic pole vibration, types of lubricant, and magnetic field strength are also investigated along with trends and capabilities in roundness and roughness.

A magnetic yoke which was supplied by T. Shinmura of Japan was assembled and adapted to fit on a Handinge precision lathe. A computer controlled system was then designed and built to operate the system, controlling magnetic field strength and the position of the magnetic poles along the workpiece. Austenitic stainless steel was used as the primary work material due to the non-ferromagnetic property of the steel, and availability of low cost ground rods.

Preliminary tests were conducted to demonstrate that structural ceramics, such

as silicon nitride, can be finished using MAF technology, to very high finish and accuracy. Due to the difficulty and expense of finishing silicon nitride by traditional methods, such as lapping and ultra-precision grinding, the MAF process offers a viable alternative to the traditional finishing techniques.

Chapter II

Literature Review of Magnetic Field Assisted Polishing

Abrasive finishing requires two things 1) pressure between the workpiece and the abrasives, 2) relative velocity between the workpiece and the abrasives. In MAF, magnetic force is used to generate the pressure between the work and the abrasives by generating a magnetic field gradient component which is perpendicular to the surface of the workpiece. The resulting force may be calculated by

$$F=\mu_0 V\chi H\frac{dH}{dx}$$

where F is the force in the x direction, μ_0 is the permeability of vacuum, V is the volume of the particle, and H is the magnetic field strength. In the arrangement used to finish cylinders in this investigation, rotation of the workpiece provides one velocity component which is in the circumferential direction with respect to the workpiece, and vibration of the magnetic poles or workpiece provides a second velocity component in the direction axial to the work. The result is an "S" shaped path of the abrasive particles on the surface of the work. The arrangement used in the present investigation is illustrated in Figure 2.1.

There are three essential parts in a MAF machine: 1) Mechanism for magnetic

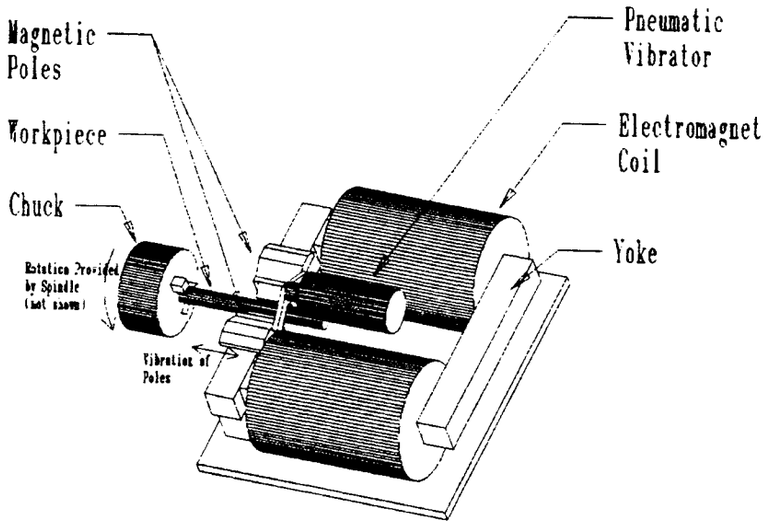

Figure 2.1: Schematic diagram of MAF attachment used in this investigation.

field generation, 2) ferromagnetic abrasives, and 3) the workpiece. The arrangement of these three components is dependent on the shape of the component to be finished, and the field distribution desired. The arrangement must be such that the conditions for finishing mentioned above, pressure and relative velocity between the work and abrasives, are achieved. The following is a brief review of the technical literature, illustrating some arrangements for MAF. Not only are techniques of finishing rods described, but finishing of tubes and plates is also included to demonstrate the principles associated with the MAF process.

One of the first uses for magnetic abrasive finishing was patented by Coats in 1940 [Coats, 1940] and is illustrated in figure 2.2. Coats used magnetic abrasives to clean the inside of drums. This arrangement is perhaps the most intuitive design for MAF of a component. This technique uses magnetic abrasives inside the barrel, or drum, which are pulled toward the inside wall of the drum by a magnetic field, while the drum is rotated with respect to the magnetic poles.

The concept used by Coats to clean drums has been further developed by other researchers to finish the inside of non-ferromagnetic tubes [Baron, 1986, Shinmura, 1986, 1988]. Simply by using higher rotational speeds and more advanced magnetic abrasives than those used by Coats in 1940, the technique may be used today to finish a variety of materials, from copper pipe to ceramics. Not only may straight tubes be finished, but by rotating the magnetic field, as opposed to the workpiece, components such as pipe elbows may be readily finished by this process. The techniques for generating a rotating magnetic field include: 1) rotating permanent magnets and 2) electromagnetic poles which are energized by multi-phase current [Shinmura 1986], for example, 3 poles located

120 degrees apart around the workpiece energized by three phase current.

It is important to note that in this technique, the magnetic abrasives are pulled towards the magnetic poles, and the workpiece, by the same component of the magnetic field since the workpiece and the magnetic poles are in the same direction with respect to the magnetic abrasives. This situation is not true in the case of finishing non-ferromagnetic cylinders, which will be pointed out later.

MAF techniques may also be employed to finish flat or curved plates. For example Shikhirev et al. of the former USSR used a MAF technique to finish flat sheet materials, such as printed circuit boards [Shikhirev et al., 1980]. The designs by Shikhirev are illustrated in Figure 2.3.

The arrangement used by Shikhirev employed rotating magnetic poles, one of each polarity, which are placed along side one another leaving a thin gap. Magnetic abrasive powder is placed between the poles, which results in the generation of a magnetic brush between the poles. The poles are then rotated and the workpiece is fed between the poles, through the abrasive brush. The potential of supplying fresh abrasives to the area being finished was one of the capabilities of MAF of which Shikhirev took advantage. The first attempt of abrasive circulation included spiral grooves on the rotating poles, which caused the abrasives to circulate, thus exposing fresh abrasives to the workpiece. The second iteration included electromagnetic poles, which may be switched off to release the abrasives, which could then be recirculated or discarded. The workpiece may also serve as a magnetic pole when finishing surfaces. Such work has been done by Anzai et al. of Japan to finish dies [Anzai et al., 1993].

MAF has been used in the past to finish ferromagnetic cylinders [Shinmura, 1989,

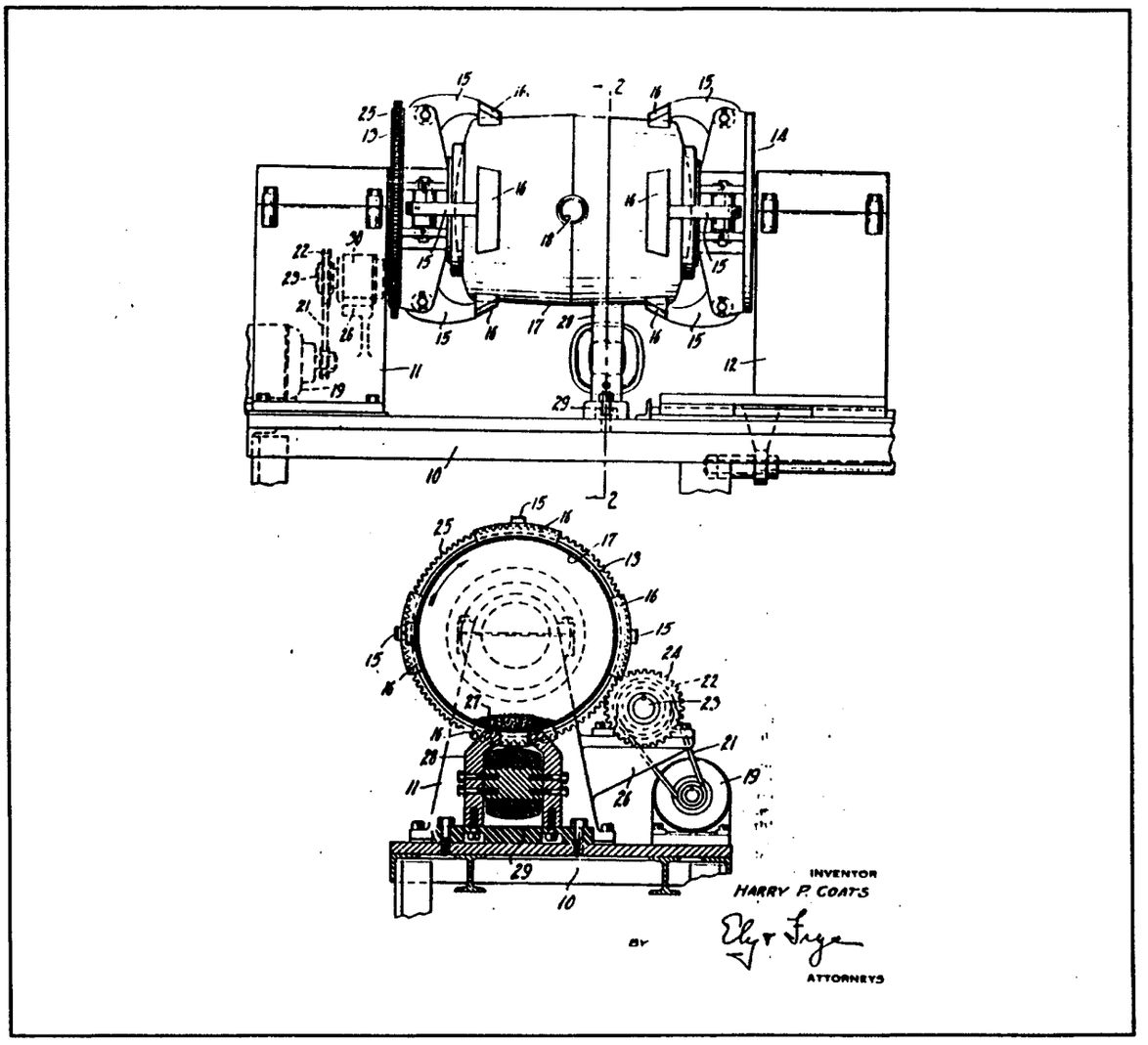

Figure 2.2: Arrangement used by Coats in 1940 to polish or clean the inside of containers (source: Coats, 1940)

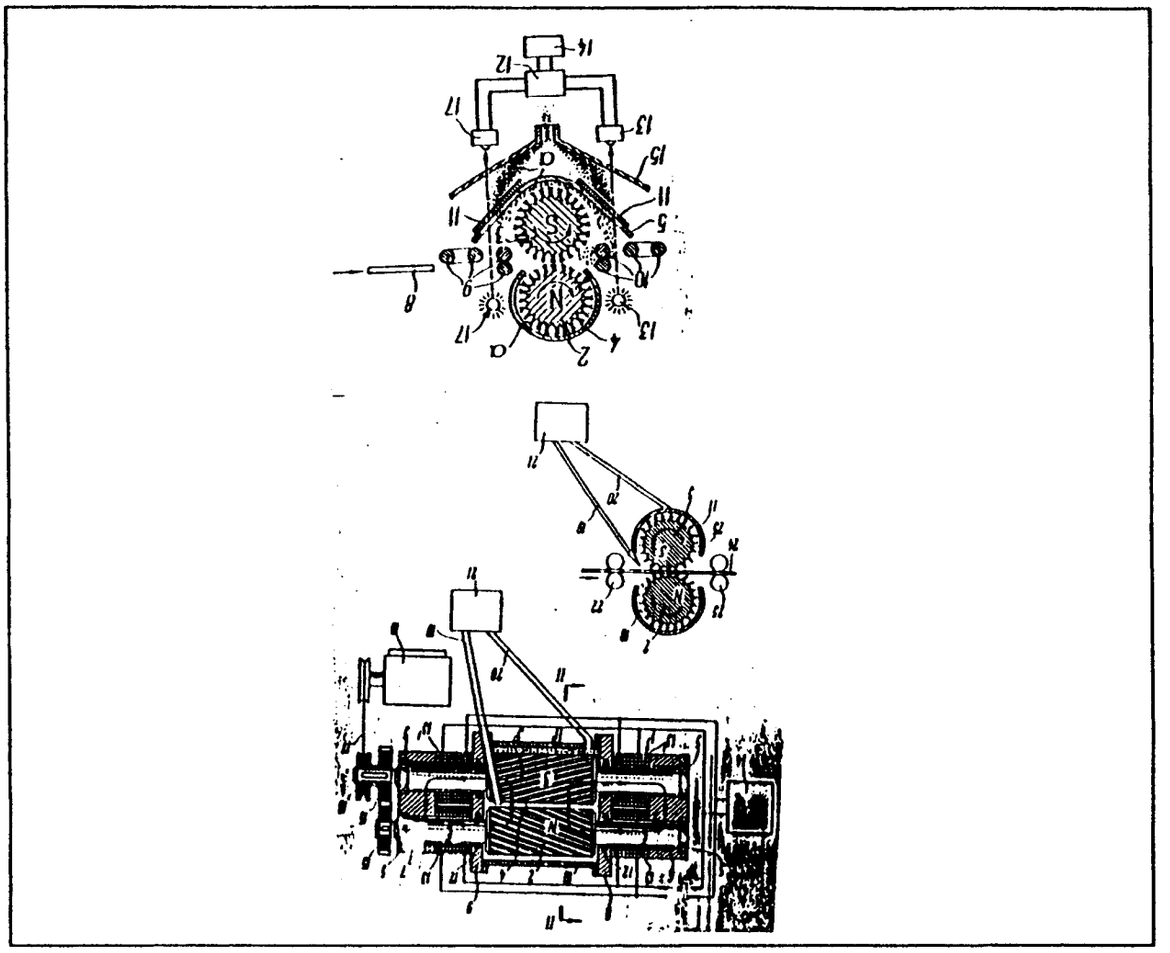

Figure 2.3: Arrangement used to finish sheet material. Front and side views (top and center) Abrasive recirculation scheme (bottom). (source: Shikhierv, 1977, 1980)

Baron, 1986]. Figure 2.4 illustrates an arrangement for finishing magnetic materials using the MAF process. This technique is similar to that used by Shikhirev in the respect that the workpiece is placed inside a magnetic abrasive brush which is formed between magnetic poles. In this arrangement a magnetic workpiece is placed between magnetic poles, providing a low magnetic resistance flux path through the workpiece. The abrasive particles are then magnetically forced to the regions of highest magnetic flux, which forms a magnetic brush between the workpiece and the magnetic poles. The workpiece is then rotated, providing the relative velocity, which may be accompanied by axial vibration of the workpiece or magnetic poles which provides a second velocity component. Since the resistance of the magnetic "circuit" is mostly due to air-gaps, the resistance of this arrangement is fairly low. The low resistance is a result of the ferromagnetic workpiece being part of the magnetic circuit, resulting in only a very small gap, of the order of 1 mm, between the workpiece and the magnetic poles.

When a non-ferromagnetic workpiece is used, the resistance of the magnetic flux path increases due to the low permeability of the workpiece. The permeability of a non-ferromagnetic workpiece is comparable to that of a vacuum, as opposed to that of a ferromagnetic material which may have a magnetic permeability several thousand times higher than that of a vacuum. For this reason, under similar conditions, magnetic flux density is significantly higher in the case of the ferromagnetic workpiece. A general representation of magnetic flux paths in the case of ferromagnetic and non-ferromagnetic materials are shown in Figure 2.5. Notice that not only the distribution of magnetic flux differs, but the gradients are much higher in the case of the ferromagnetic workpiece. The higher flux densities along with the higher flux gradients results in higher forces, thus

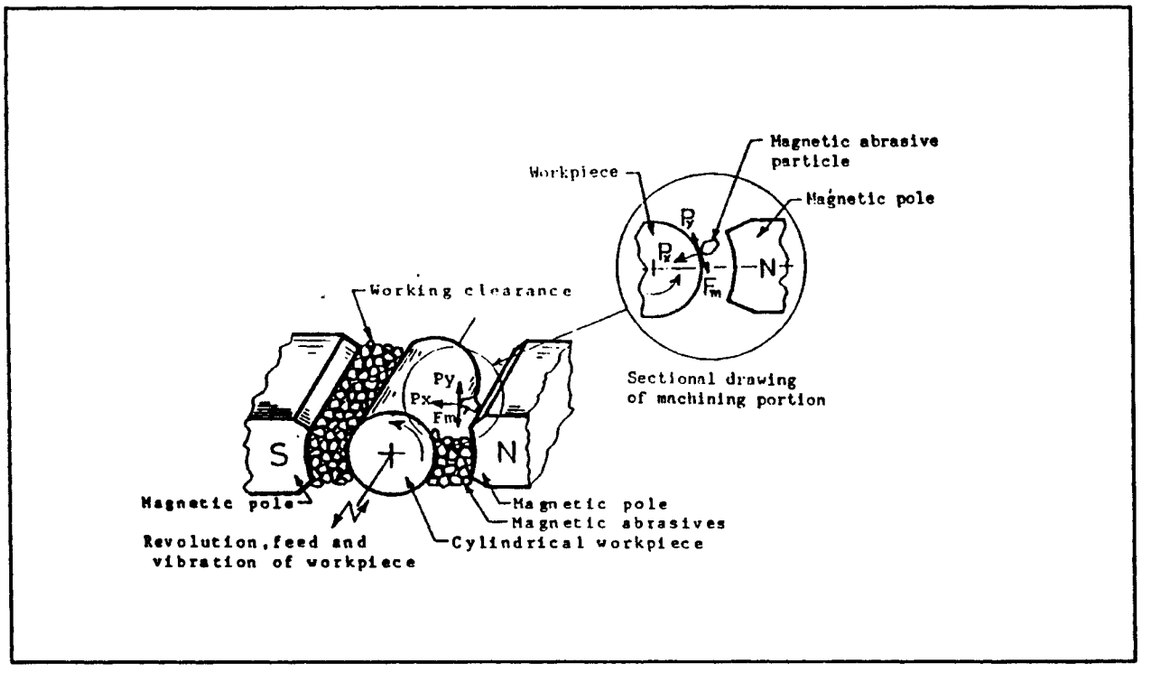

Figure 2.4: Arrangement for finishing ferromagnetic cylinders in the case of vibrating workpiece. (source: Shinmura, 1989)

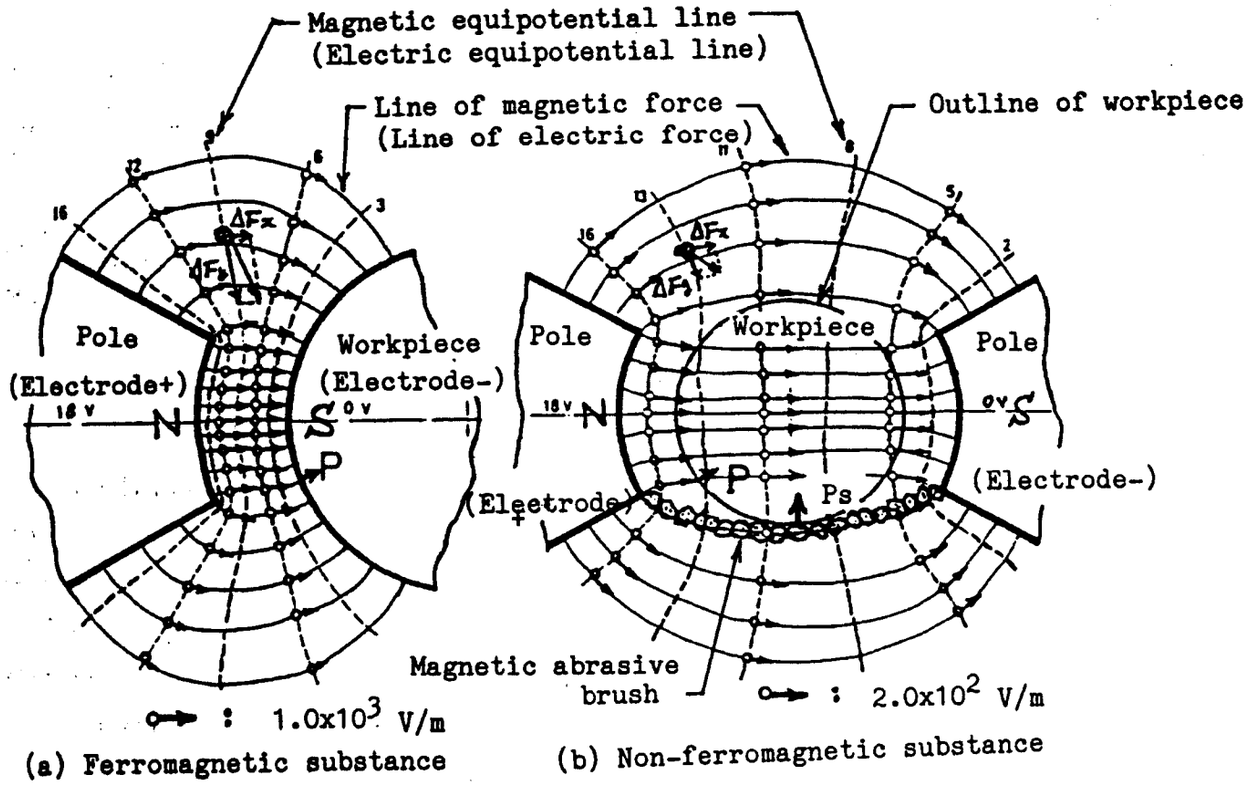

Figure 2.5: Two dimensional magnetic field distributions simulated by electric field distributions. (source: Shinmura 1990)

higher finishing pressures in the case of the ferromagnetic workpiece.

Figure 2.6 illustrates some quantitative differences in forces, comparing ferromagnetic and non-ferromagnetic materials. These results show that forces generated in the case of a ferromagnetic workpiece are around three times that of the forces obtained when a non-ferromagnetic workpiece is used. The forces generated in the case of the ferromagnetic workpiece are also a strong function of the working clearance, which is the distance between the workpiece and the magnetic pole. This is because the magnetic flux resistance of the working clearance is a major contributor to the total resistance of the flux path. However, in the case of a non-ferromagnetic workpiece, the resistance of the total path is much higher, and as shown in Figure 2.6, a change in working clearance does not significantly change the resulting forces.

The shape of the magnetic poles influences the magnetic flux distribution around the workpiece. Shinmura et al. have conducted several investigations on the effect of magnetic pole shape on material removal rates in the case of ferromagnetic, and non-ferromagnetic materials [Shinmura, 1987]. This study indicated that the magnetic pole shape which results in high material removal rates for ferromagnetic materials is not necessarily the best pole shape for non-ferromagnetic materials [Shinmura, 1987]. Figure 2.7 shows three magnetic pole shapes, along with the material removal obtained after 4 minutes finishing time. The work material is brass, 20 mm diameter, and is used to represent non-ferromagnetic materials. The results indicate that design II is the best pole shape for high material removal rates. The majority of the magnetic flux between the magnetic poles takes place between the two closest points between the two poles. Therefore, if the poles are close together, the magnetic resistance is low and high flux

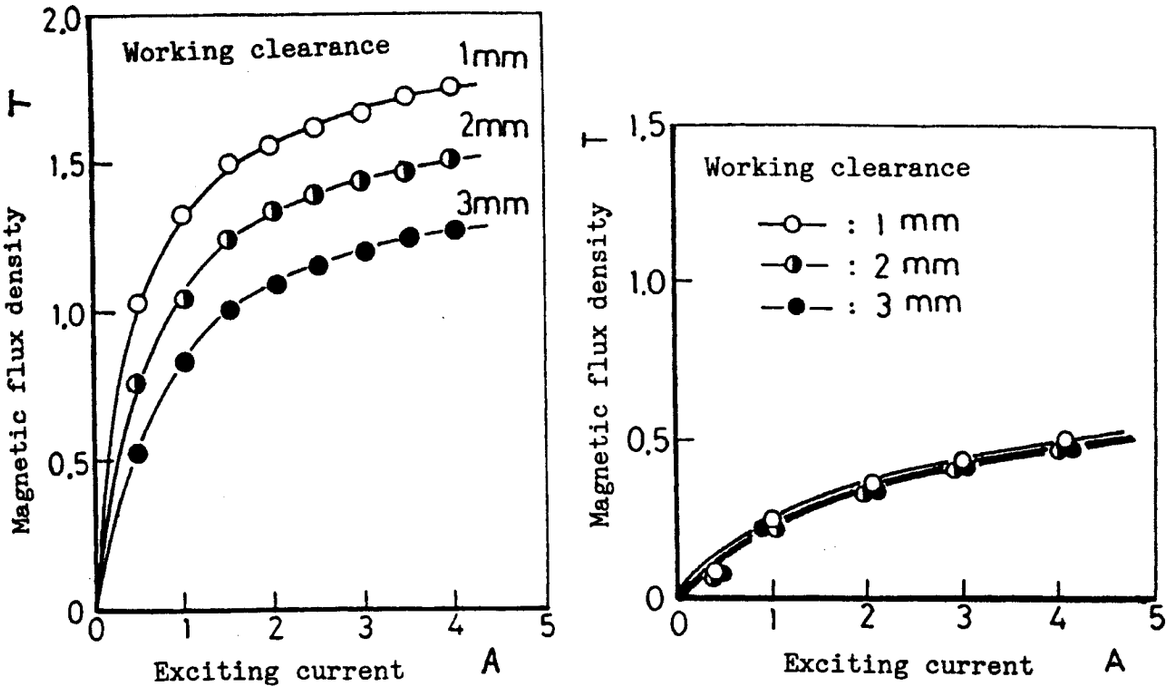

(a) In the case of ferromagnetic substance (dia. = 30mm)

(b) In the case of non-ferromagnet: substance (dia. = 20mm)

Figure 2.6: Relationship between magnetic flux density and exciting current for ferromagnetic and non-ferromagnetic materials. (source: Shinmura, 1990)

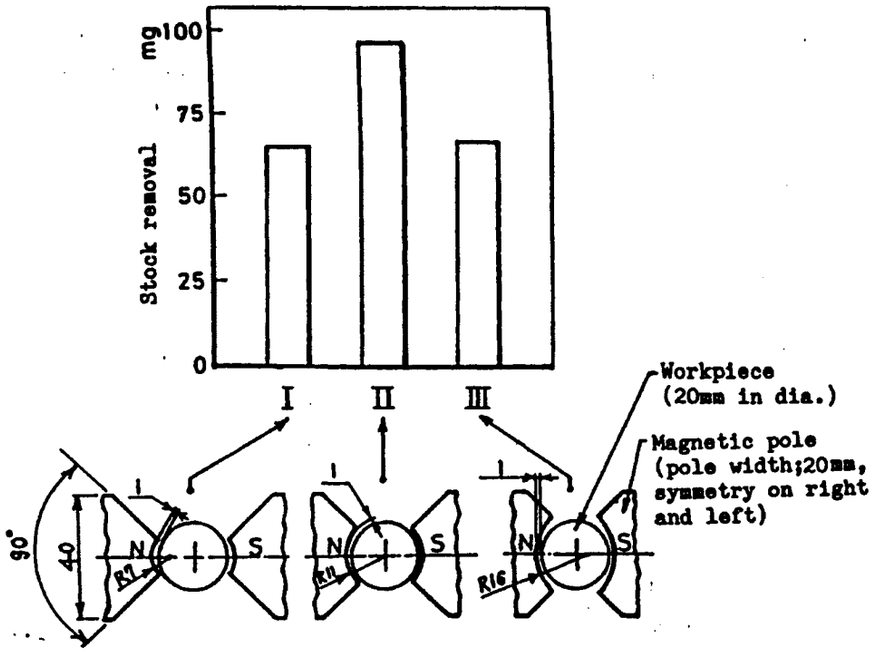

Figure 2.7: Effect of pole shape and its size on stock removal in the case of non-ferromagnetic workpiece. (source: Shinmura, 1990)

densities may be obtained which results in high forces. If the magnetic poles do not extend around the workpiece as shown in design I, a high resistance and low flux densities result. The result obtained by Shinmura imply that the magnetic pole should be contoured as to fit around the workpiece, with each pole covering around 1/4 of the circumference of the workpiece.

Chapter III

Work Materials and Magnetic Abrasives

In this chapter the work materials are discussed first, followed by magnetic abrasives. Although stainless steel is the work material used in this investigation, the ultimate goal of this project is to finish other non-ferromagnetic materials such as silicon nitride. It is therefore necessary to examine not only at the properties of stainless steel, but also of silicon nitride which will help drive the technology toward the finishing of advanced ceramic materials. First, stainless steel material is discussed. This includes the composition and magnetization of stainless steel, followed by the selection of a nonmagnetic stainless steel to simulate the magnetic property of ceramic materials. Next, silicon nitride material is discussed, from composition and fabrication, to finishing methods including mechano-chemical material removal.

The next topic of this chapter is magnetic abrasives. Types of magnetic abrasives along with brief descriptions of fabrication techniques are reviewed, followed by a description of the abrasive particles used in this investigation.

3.1 Stainless Steel

Stainless steels are iron-based alloys which contain from 10.5% to 30% Cr and from 0.03% to 1.0% carbon. Stainless steels form an adherent chromium rich oxide

protective surface film which gives them their "stainless" property in the presence of oxygen. Elements such as nickel, molybdenum, titanium, aluminum, silicon, niobium, nitrogen, sulfur, and selenium are often added to alter the properties of the steel [Washko et al., 1990]. There are five major groups of stainless steels: martensitic, ferritic, austenitic, duplex, and precipitation hardening stainless steels.

3.1.1 Non-ferromagnetic Stainless Steel

Of the stainless steel types, only the austenitic stainless steels are non-ferromagnetic, which is a requirement for this research. This is because although polishing of stainless steel in itself is of great commercial interest, we are ultimately interested in finishing advanced ceramics for ARPA ceramic bearing technology program. Alloying elements of austenitic stainless steels includes 16% to 26% chrome, around 35% nickel, and up to 15% manganese. The 2xx series contains nitrogen, 4 to 15.5% Mn, and up to 7% Ni. The 3xx series contains more nickel and less manganese than of the 2xx series.

The stainless steel used in this investigation is 303 (UNS S30300) austenitic stainless steel. This alloy contains 0.15% C, 2% Mn, 1% Si, 17% - 19% Cr, 8% - 10% Ni, 0.20% P, 0.15% S, and may contain 0.6% Mo. This type of stainless steel contains 0.15% S which improves machinability. The supplier for this material is W.M. Berg, Inc. (East Rockaway, NY). Berg part number S8-60 was used in this investigation which is a 1/2" x 6" (1.3 cm x 15.2 cm) ground shaft (303 stainless) with a nominal surface finish of 12 μin Ra (0.3 μm Ra). Actual surface finishes of the bars are usually around 0.2 μm when measured for use in this investigation. This specific material was chosen due to it's

nonmagnetic property, convenient size, and availability at reasonable cost.

3.2 Silicon Nitride

As already pointed out, although stainless steel is the principal work material used in this investigation, the ultimate goal of this research is finishing silicon nitride rolling elements for use in roller bearings. For this reason, a review of silicon nitride material is given. It includes information which may be relevant to the finishing of this material, such as composition, structure, and surface properties. Mechano-chemical material removal is briefly discussed since this "non-traditional" method of material removal may be useful when finishing advanced ceramics.

3.2.1 Structure of Silicon Nitride

Based on the model presented by McColm [McColm, 1983] the heart of the structure of silicon nitride is the silicon atom. The electron configuration of the silicon atom encourage covalent bonding of the silicon atom with four nitrogen atoms. The silicon and nitrogen atoms form a SiN_4 tetrahedron which becomes the building block of silicon nitride. Once the SiN_4 tetrahedron is formed, silicon atoms become attached to each of the four nitrogen atoms. The new silicon atoms each have three free bonding sites for nitrogen atoms. Nitrogen atoms bond to these free sites and the cycle continues to repeat, forming a matrix of Si_3N_4. Since every silicon atom is predominately covalently bonded with four nitrogen atoms, and every nitrogen atom is covalently bonded with two silicon atoms, a very rigid structure results.

Pure silicon nitride has only one crystal structure which is termed β-Si_3N_4. The

structure was termed the β-phase because it was believed that another morphology, namely α-Si_3N_4, existed. The α phase is presently considered to be an oxynitride. In this oxynitride structure, oxygen replaces approximately one of every 30 silicon atoms, and one in every 120 silicon sites are left vacant to achieve electric neutrality. This structure is non-stoichiometric and may range from $Si_{11.4}N_{15}O_{0.3}$ to $Si_{11.5}N_{15}O_{0.5}$, an average of $Si_3N_{3.9}O_{0.1}$ is sometimes assumed.

In the process of preparing β-Si_3N_4, a layer of silicate is unavoidable on the surface of the silicon before preparation. For this reason it is suggested that $Si_3N_{3.9}O_{0.1}$ is the initial building block of β-silicon nitride. Therefore silicon nitride begins as an α-phase and shifts to β at around 1300C. Since SiO is evaporated from the system during the α to β transition, the transition is irreversible and remains in the β-phase. Figure 3.1.1 represents the silicon-nitrogen-oxygen system as presented by McColm while I have added the α and the SiO phases to complete the diagram.

3.2.2 Fabrication of Silicon Nitride Components

Silicon nitride can be formed by a number of methods, some of which are listed below:

$3Si + 2N_2$ ----1400C----> Si_3N_4

$3SiO_2+6C+2N_2$ ----------> $Si_3N_4 + 6CO$

$SiCl_4+6NH_3$ ----- 0C -----> $Si(NH)_2 + 4NH_4Cl$

$nSi(NH)_2$ ---360C----> $[Si(NH)_2]_n$ ----1200C----> α-Si_3N_4

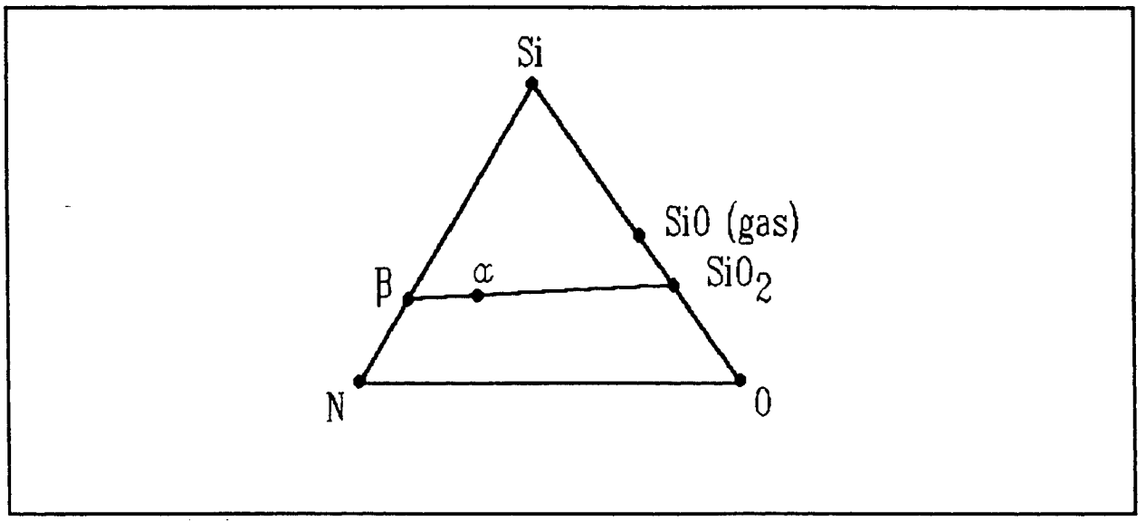

Figure 3.1.1: Silicon-nitrogen-oxygen system.

Because silicon nitride is covalently bonded and also does not have a large number of vacancies, high density (>99% dense) silicon nitride can not be produced by sintering alone. The material may be formed by hot pressing, reaction bonding, vapor deposition warm molding or foaming.

The first method of silicon nitride component formation is hot pressing or hot isostatic pressing (HIP) and is usually the process of choice for structural applications of silicon nitride. In the hot pressing procedure silicon and nitrogen are reacted at 1400C to form α-silicon nitride powder. The silicon nitride powder is then mixed with densification aids, discussed later, and the mixture is subjected to 20 MPa pressure at a temperature of 1700C. After around 30 minutes the transition from α to β is complete and silicon nitride components with very high density(>99%) results.

3.2.3 Additives

Sintering of silicon nitride takes place in three stages:

1. Particle rearrangement
2. Solution of α-phase and precipitation of β-phase
3. Coalescence

If all three of these stages are to be achieved there must be an appreciable liquid phase present which will completely wet the α phase of silicon nitride. When hot pressing silicon nitride, densification during sintering does not occur unless additives such as magnesia, yttria, or zirconia are present. These additives help the silicon to form a liquid

form which is necessary for sintering. Since silica becomes "liquid" at 1700C, the silica may help in the sintering process. However, silica reacts with Si_3N_4 to form oxynitrides before it can take part in the sintering process.

The first additive used for sintering of silicon nitride is MgO, which is the additive used for the silicon nitride used in this investigation. MgO reacts with the silica layer on the Si_3N_4 to form a silicate liquid near the $MgSiO_3$-SiO_2 eutectic point. The reaction then continues to form an Mg-Si-O-N glass which can wet the α-phase of silicon nitride. β-phase silicon nitride can then be precipitated and a glassy layer is formed in the resulting grain boundaries. This glassy layer results in reduced strength at elevated temperatures due to glass flow.

The second additive used is Yttria (Y_2O_3). Yttria reacts with silica and Si_3N_4 to form a liquid phase which aids in the α to β phase transition. Yttria then forms a refractory grain boundary phase which results in higher strength than that of the glass phase left in the case of MgO. However, the refractory phase may be subject to oxidation at high temperatures. The resulting volume change will cause the component to fail due to cracking at the grain boundaries. Oxidation may be avoided if careful attention is given to keeping the stoichiometry in the Si_3N_4-Si_2N_20-$Y_2Si_2O_7$ compatibility triangle.

The third additive is Zirconia. ZrO_2 works in much the same way as yttria, forming a liquid phase which dissolves the α-silicon nitride. The products left in the grain boundaries are also subject to oxidation if outside the Si_3N_4-Si_2N_2O-ZrO_2 compatibility triangle.

The second method of silicon nitride component formation is reaction bonding. The reaction bonding process has the advantage of being able to make more complex

shapes than hot pressing. The process begins by pressing silicon powder into the desired shape. The shaped part is then placed in a furnace and heated to 1400C in a N_2 atmosphere. The nitrogen then reacts with the silicon to form a mixture of α-phase and β-phase silicon nitride with around 25% porosity. The beginning of the reaction is dominated by α-phase formation. After two hours β-phase formation begins to dominate. The end result is a mixture of 20% α and 80% β-phase morphology after about 20 hours. As mentioned, the α-phase is a result of oxygen in the SiO_2 coating on the surface of the silicon. Some of the silica layer may be removed by adding 2% of metal fluorides to the silicon. This fluoride addition results in higher growth rates and a lower α-phase to β-phase ratio.

3.2.4 The Surface of Silicon Nitride

The surface of silicon nitride is quite complex and chemically active. The cause of this chemical activity is dangling bonds at the surface of the silicon nitride. Since every silicon in β-silicon nitride favors bonds with four nitrogen atoms which in turn favor being bonded to two silicon atoms, bonding is incomplete at the surface of the β-silicon nitride crystal. The resultant open bonds make the surface quite active. The machining process may start a cycle of new surface generation, surface reaction, surface removal, etc. Although the exact nature of the resulting chemical reactions on the surface of silicon nitride is unknown, several possibilities exist which may facilitate the machining process.

In the presence of oxygen open silicon bonds may react with oxygen to form $Si_xN_yO_z^{(charge)}$ or other arrangements. As a result the surface of the crystal may become charged and thus attract anions to balance the surface charge, or a positively charged atom

must be forced from the lattice. In the case of silicon nitride the positive atom is Si^{4+}. When the silicon finds its way to the surface it is free to bond with compatible materials in the vicinity. One common result is the formation of silicate groups when oxygen is present.

When silicates form, the surface chemistry becomes quite complex. This is due to silicates not only forming SiO_4^{4-} groups, but silicates with other structures are also very common [Evans, 1964]. Silicates often substitute other species for the silicon and oxygen atoms. Ions such as Mg^{2+}, Fe^{2+}, Na^{+}, and Ca^{2+} often periodically replace the silicon atom and species such as O^{2+}, OH^{-}, and F^{-} may replace the oxygen. The aluminum ion is also important to silicate formation. Since the Al:O atomic radii ratio is close to the critical value which allows 4 oxygen ions, instead of 6, to pack with the aluminum ion. Every time an aluminum ion packs with an oxygen co-ordination number of 4, another ion in the lattice must be replaced with an ion of one less positive charge to balance the charge in the lattice. Chemical structural analysis of the surface of silicon nitride is almost impossible, and as a result, interpretation of silicate structures is very difficult. Therefore, surface chemical structural characterization of silicon nitride can be hypothesized, but is very difficult to prove.

Orthosilicate groups are those silicates which result from isolated SiO_4^{4-} species which are interconnected by cations. The following are examples of the resulting structures.

Perhaps the simplest structure is forsterite, Mg_2SiO_4 which is an olivine structure. In this structure the SiO_4^{4-} tetrahedra alternate pointing up and down. The Mg^{2+} ions then form O-Mg-O bonds to link the structure. Other similar structures result from the Mg^{2+}

ion being replaced by Fe^{2+}, or Mn^{2+} which form Fe_2SiO_4 and Mn_2SiO_4 respectively.

Soft silicates are formed when silicate structures are held together only by van der Waals forces in at least one direction. The result is the formation of sheets which may be easily removed. One such structure is talc. Talc is $Mg_3(OH)_2Si_4O_{10}$. This can be represented by $MgO_4(OH)_2$ and SiO_4 tetrahedra which are joined together by sharing oxygen atoms. The second soft structure are the clays. The clays are similar to talc in structure. For example kaolinite, $Al_2(OH)_4Si_2O_5$, may be represented by $AlO_2(OH)_4$ octahedra joined to SiO_4 groups by sharing oxygen atoms and forming sheets, again held together only by van der Waals forces.

The material presented in this section is only a brief summary of silicate structures, and most is based on the work of R. C. Evans [Evans, 1964]. For more details, one may refer to the reference cited.

3.2.5 Mechano-chemical Polishing

Mechano-chemical polishing is a combination of chemical and mechanical material removal. There are several reasons why the combination of chemical and mechanical reactions are useful in the material removal. First, the rate and path of chemical reactions may be influenced by simultaneous occurrence of friction and impact [Fisher 1988]. Since ceramics are prone to brittle fracture under machining loads, chemo-mechanical material removal may provide an alternative method which does not result in fracture and degradation of the surface. In fact the surface may even be left virtually scratch free if the abrasive is softer than the workpiece[Vora *et al*, 1982] which is possible using mechano-chemical techniques.

Although silicon nitride is covalently bonded, it has some degree of ionic bonds also. Evans gives an analytical method to calculate the degree of ionic bonding of a binary material based on electronegativity. The relation is

$$p = 16 |x_a - x_b| + 3.5 |x_a - x_b|^2$$

where p is the percent of ionic bonding and x_n is the electronegativity of the element n. In this case the two elements are, of course, silicon and nitrogen.

For β-silicon nitride, the following results

$$p = 16 |1.8 - 3.0| + 3.5 |1.8 - 3.0|^2 = 19.20 + 5.04 = 24.24$$

where 1.8 and 3.0 are the electronegativities of silicon and nitrogen respectively [Evans 1964]. The result is that β-silicon nitride has around 24% ionic bonds and 76% covalent. Ionic bonds which are weaker than covalent bonds give silicon nitride the opportunity to be more chemically active than if it had all covalent bonds.

As mentioned in Section 3.2, silicon nitride also has a glassy surface which is the result of oxygen bonding with exposed silicon forming $Si_3N_3O^+$. This layer is almost always present since the silicon nitride lattice is discontinuous at the surface and has open bonds which may react with oxygen. As the oxygen bonds with the silicon, an imbalance in charge results. This charge imbalance forces silicon atoms from the silicon nitride structure. The silicon moves to the surface, then reacts with oxygen forming silicates.

Perhaps the most common soft abrasive used for finishing silicon nitride is

Cr_20_3 [Uematsu et. al.]. Although the exact nature of the chemical reaction in this process is not established, chrome silicates may form, which are more easily removed from the surface by subsequent abrasive action. Uematsu used a polishing disc made of resin bonded Cr_2O_3. The results indicated that pressures above 1.3 MPa resulted in R_{max} of the silicon nitride workpiece decreasing from 170 nm to 55 nm in 30 seconds with very small if any increase in roughness due to higher pressures. Pressures less than 1.3 MPa did not result in a significant roughness decrease. The relative velocity between the workpiece and the abrasive did affect the final roughness slightly, resulting in final R_{max} values from 35 nm to 60 nm with the smooth value at higher velocities.

The second chemical reaction which can be used to finish silicon nitride is a chemical reaction with water as given by the following equations.

$$Si_3N_4 + 6\ H_2O \text{ ----> } 3\ SiO_2 + 4\ HNO_3$$

$$SiO_2 + 2\ H_2O \text{ ----> } Si(OH)_4$$

In this case the silic acid, $Si(OH)_4$, may be dissolved in water and thus removed from the surface. Note that the latter reaction may also remove the glass layer from the surface of the sample. Although chemical reaction rates usually increase with temperature, this reaction occurs more slowly at temperatures above 120C.

Iron oxides such as Fe_2O_3 and Fe_3O_4 have also been used successfully to finish silicon nitride [Vora *et al*, 1982]. Vora *et al* used iron oxides (<5μm in diameter) to finish silicon nitride to roughnesses of 20 nm Rt with no residual surface damage. It was

noted that removal rates increased with pressure up to 34.5 kPa. The resultant material removal rate was ~1.5μm/h. Auger electron spectroscopy of the resultant surface indicated a thin (<10nm) layer of silicon oxynitride with detectable amounts of carbon and around 0.5 atomic percent iron.

3.3 Magnetic Abrasive Powders

Magnetic abrasives usually contain 2 constituents: a magnetic part and an abrasive part. In some cases, the abrasive particles may be bonded to the magnetic particles (bonded type), but this is not necessary. However, it does have an effect on the finishing operation which is discussed later. Figure 3.3.1 is a schematic of a bonded type magnetic abrasive particle, showing the ferromagnetic core of diameter D, and the abrasive component of diameter d. The abrasives may also be simply a mixture of the magnetic and abrasive powders (mixed type).

There are several methods which have been used to fabricate bonded type magnetic abrasives, including sintering, attrition milling (mechanical alloying), and chemical reactions. Perhaps the most common method is sintering. The sintering process begins with a mixture of iron and abrasive (such as alumina) particles, for example 100μm Fe and 5μm alumina. The mixture is then heated to a temperature slightly below the melting temperature of iron in the presence of an inert gas such as argon. The iron then sinters to the alumina and other iron particles. The agglomeration can then be broken up and meshed to desired size. Chemical reaction type abrasives use an exothermic reaction, such as Ti + C --> TiC, in the presence of iron. The iron becomes bonded to the abrasive constituent as the reaction occurs. The agglomeration is then

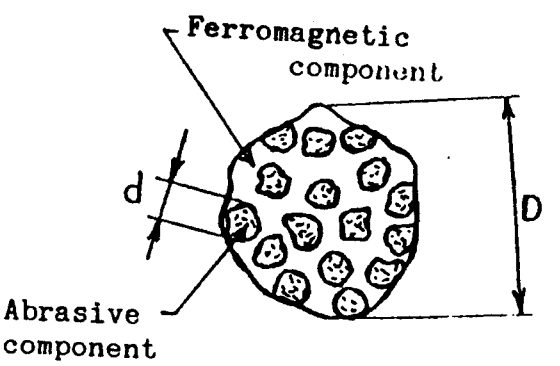

Figure 3.3.1: Schematic on bonded type magnetic abrasive particle.

(source: Shinmura, 1990)

broken apart and meshed to size.

Two types of bonded abrasive powders were used in this study: KMX 80, and M5. KMX80 and M5 abrasive are bonded type abrasives, consisting of iron and alumina. Figure 3.3.2 shows micrographs of KMX80 and M5 type abrasives, which are used in this research. The KMX 80 abrasive has a nominal diameter of 80 μm and the M5 abrasive diameter is around 200 μm - 400 μm. The size of the abrasive constituent was not determined for the KMX 80 type, but the abrasive constituent of the M5 type abrasive is 5μm.

Since there is a magnetic and abrasive components to the magnetic abrasive powders, the size of each component is significant to the finishing operation (see Figure 3.3.1). It has been proposed that the size of the abrasive grains, d, in the magnetic agglomerate is responsible for the resulting surface finish, while the size of the entire agglomerate, D, is responsible for material removal rate [Shinmura et al., 1987].

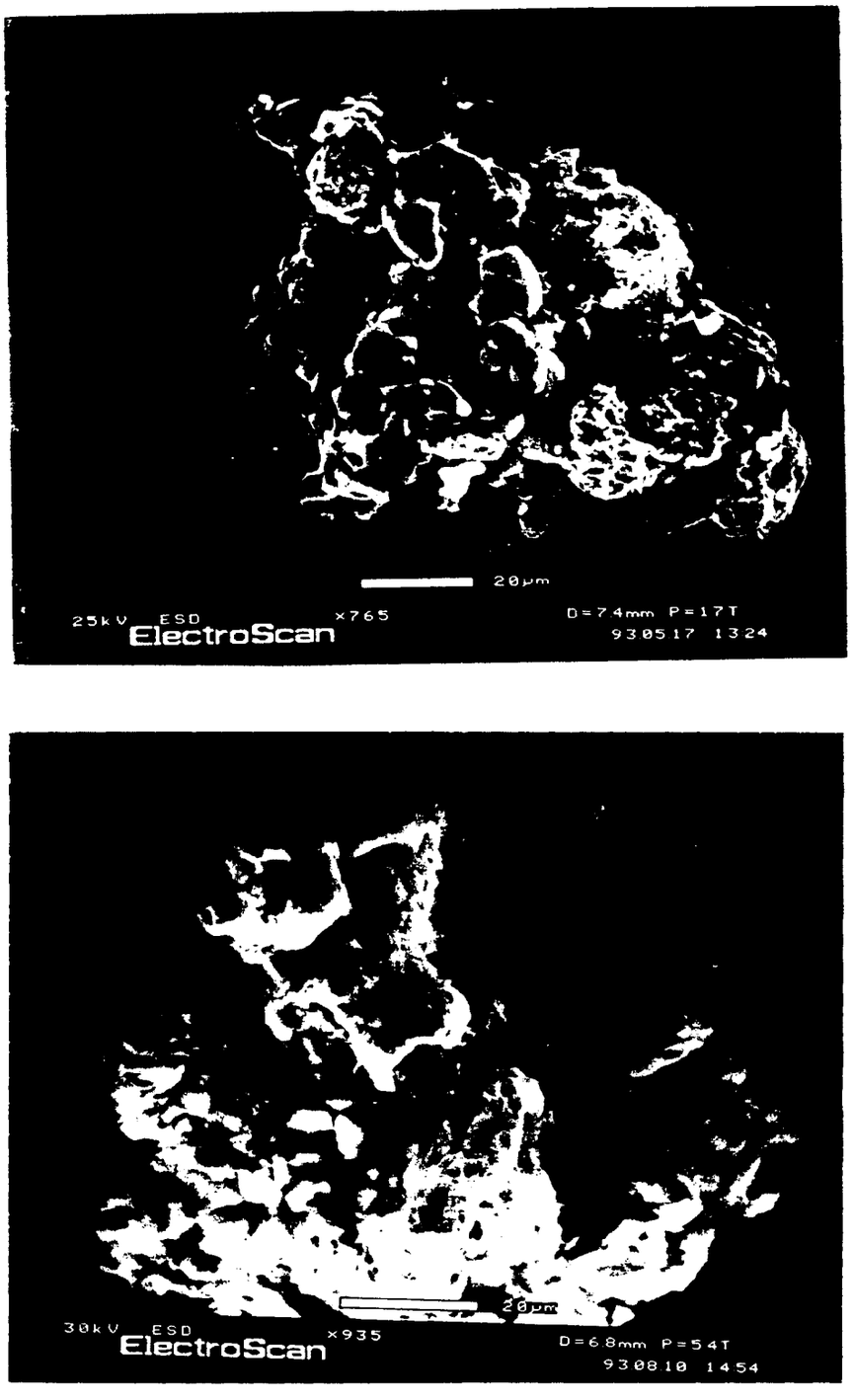

Figure 3.3.2: Micrographs of abrasives used in this study. Top: KMX 80, Bottom M5.

Chapter IV

Experimental Approach and Test Procedure

This chapter describes the experimental apparatus used in this investigation, followed by a description of the instrumentation used to characterize the samples, such as the ZYGO laser interference microscope, Talyrond roundness measuring instrument, Talysurf surface roughness measuring instrument, etc. The general experimental procedure is then discussed, which may vary slightly depending on each particular experiment.

4.1 Description of the Experimental Apparatus

The experimental apparatus used in this investigation consists of three main components. The first is the Hardinge precision lathe which rotates the workpiece. The second is the MAF attachment to the lathe which consists of the electromagnetic coils, yoke, poles, and pneumatic vibrator. The third is the electronic control system which enables a microcomputer to control the current in the coils of the electromagnet, thereby controlling the finishing pressure. The system also monitors and controls the position of the lathe carriage on which is mounted the MAF apparatus.

4.1.1 Test Equipment

The lathe used in this study is a 1120 W (1.5 HP) Hardinge precision lathe (model HLVH). The spindle speed can be varied continuously from 125 to 3000 rpm. The chuck used on the lathe is a Buck model 3525 which may be easily adjusted to center the workpiece. The spindle and chuck were replaced with new components at the beginning of this research, which ensured rigidity and accuracy of the system.

The MAF apparatus, mounted on the carriage of the lathe, is shown in Figure 4.1.1.1. It is basically a "U" shaped electromagnet which has vibrating magnetic poles. The yoke of the electromagnet is constructed from low carbon steel, approximately 20 mm square.

The poles of the electromagnet are mounted on linear ball bearings. This enables the poles, which are the polishing heads, to vibrate in the axial direction of the workpiece. Vibration of the poles is actuated by a pneumatic vibrator which is capable of supplying 15 to 30Hz when supplied with 700 kPa (100 psi) air.

The coils which supply the magnetic field to the system are 70 mm in diameter and are 200 mm in length, with a 70 mm diameter iron core in the center. The copper wire used in the windings of the coil has an approximate diameter of 1.4 mm. Taking the area of the coil equal to the area of the wire results in approximately 5000 turns per coil. Adjusting this figure by multiplying by 0.8 to allow for loose windings, 4000 turns per coil results. The 4000 turns in the coil, current through the coil, and the overall resistance of the magnetic flux path, determines the strength of the magnetic field. Appendix I gives more information on the magnetic field calculations.

The electronic control system is designed primarily to control the voltage, thus

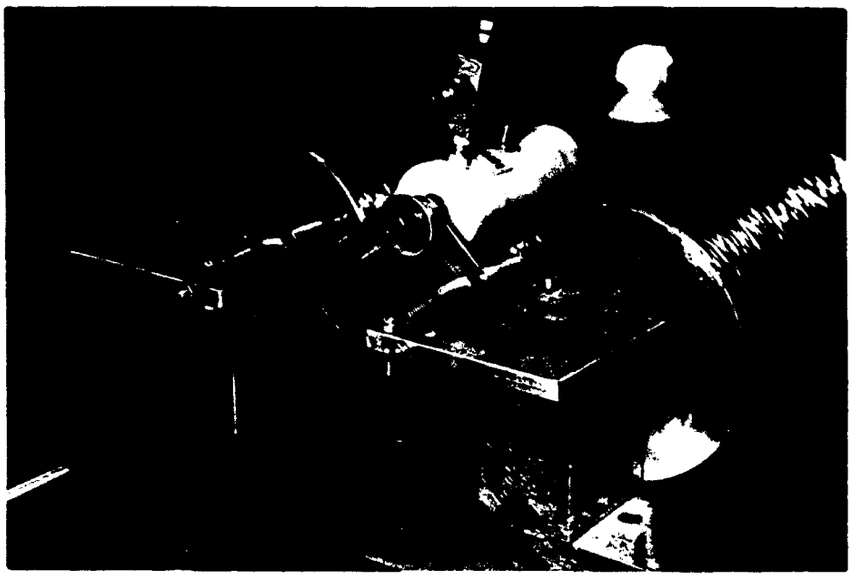

Figure 4.1.1.1: MAF apparatus used in this investigation.

current, to the coils of the electromagnet automatically. Secondary functions include monitoring the position of the lathe carriage, and providing two high power switcheswhich may be used to control the position of the lathe carriage, on/off of the pneumatic vibrator, or any other desired function. The computer may also be used to time experiments, keeping track of total run time and run time intervals. Schematics of all electronics built for this research are given in Appendix II, as well as the source code written to control the system.

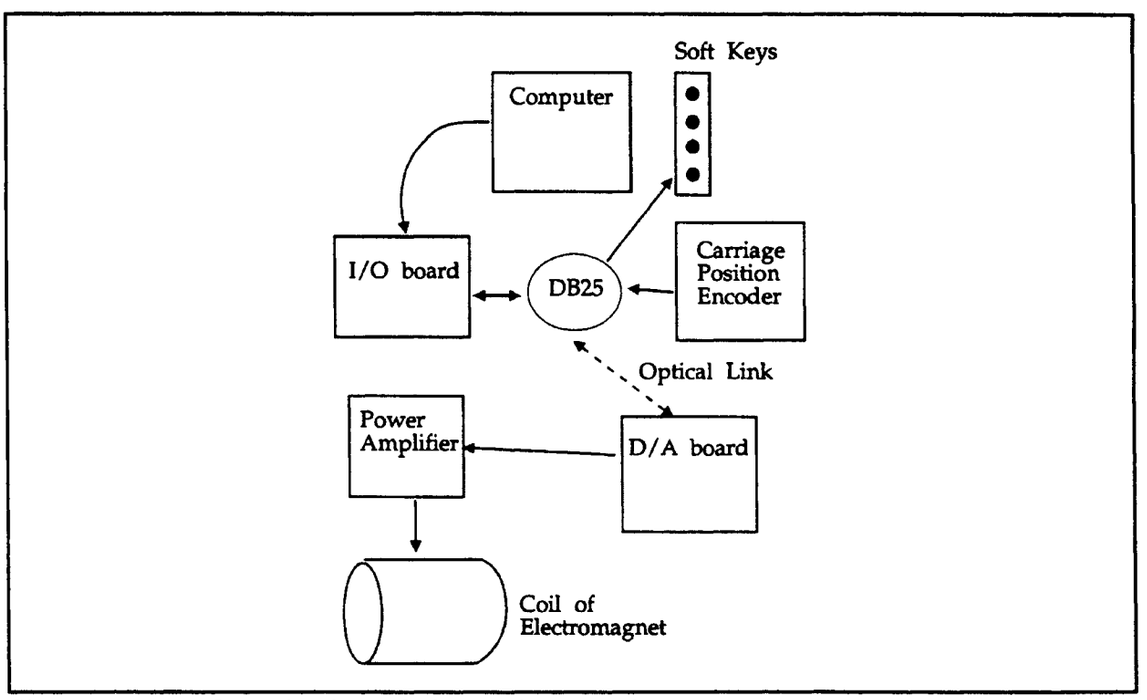

Figure 4.1.1.2: Organization of electronic control system

The electronic control system is controlled by an 8088 based microcomputer. The 8088 based PC offers enough computational power and speed to control the system while also remaining cost effective, which is an important consideration when building prototype equipment where the computer may be damaged during construction and testing. A

schematic showing the organization of the electronics built for this investigation is shown in Figure 4.1.1.2. The following is a description of the interface.

The system is controlled by a set of 5 soft menu keys, which are buttons mounted on the right side of the monitor who's function is displayed on the monitor next to the keys. This allows the function of each button to change as needed, thus eliminating the need for a keyboard on the system.

All input and output goes through an 8255 chip. The 8255 is a chip which has three sets of eight bit I/O ports which can be configured for either input or output. These three digital ports handle all input and output between the computer and the MAF equipment. In the configuration used in this system, two ports are configured for output, and the remaining port is used for the input. The computer communicates with the 8255 chip through two address lines, eight I/O lines, and a few other support connections. The two address lines enable the computer to actually address four addresses, the fourth address is the configuration port, writing to this location configures the chip and tells it which ports are inputs etc.

From the 8255 information leaves through a DB25 connector, which is a 25 pin connector whose pins are referenced from DB1 to DB25. The data is distributed to and from the soft keys, carriage position encoder, and D/A board from this connection.

The carriage position encoder is capable of resolving the position of the lathe carriage to 2.54 mm. This is done by positioning a thin strip behind the carriage which has holes drilled in staggered rows along the strip. As the carriage moves, a strip of inferred emitter-detector pairs moves along the encoder strip which causes the detector to periodically detect the infrared signal. The computer watches the pattern of detected

light signals and is able to detect a movement of 0.1 inch and the direction of the movement, which enables the position of the carriage to be monitored.

The soft keys, which are mounted on the side of the monitor, are simply a series of momentary push button switches. The signal from these buttons are fed through the DB25 directly to a port on the 8255 which digitally indicates when a button is pressed.

The remaining connections go through an optical link which isolates all power sources on the remaining circuits from the computer. This is done because the remaining power may be noisy, and may be accompanied by power surges which may damage the computer. Optical isolation is performed by a series of 4 channel chips, specifically referenced as 2506's.

Connected to the optical data link is the digital to analog convertor. This chip takes an eight bit input (0 to 255) and converts the signal to analog 0 V to -2.5 V in this particular configuration. The analog signal is then passed to a high power amplifier (Apex PA01 or PA12, the latter handling more power), which converts the analog signal to 0 V to 24 V capable of delivering up to 6 A. This voltage may be increased by switching on an auxiliary power supply which adds 24 V to the system. The output is now 0 V to 48 V at up to around 6 A. This power is ran through the coils of the electromagnet, which are connected in series, and a magnetic field is generated.

The system does have the ability to sink two currents to ground via a pair medium power transistor (~2 A) which may be switched on or off by the computer. This switching system may be connected to two relays, one of which may switch on and off the power to the electric carriage driving motor and the other switching the polarity of the input power to the driving motor, thereby controlling the direction of travel. This system

coupled with the carriage position encoder allows the carriage to be automatically positioned if desired. The relays may also be connected to other devices such as the solenoid which controls the air pressure to the pneumatic vibrator, thus enabling the vibration to be switched on and off via computer.

4.2 Surface Characterization Instrumentation

4.2.1 Talyrond 250

The Rank Taylor Hobson Talyrond 250 is used to measure the roundness of the samples. The talyrond is a computer controlled stylus type instrument which measures geometric form such as roundness or straightness. Evaluations which are returned by the instrument include roundness, straightness, squareness, parallelism, flatness, co-axiality, cylindricity, concentricy, eccentricity, runout, and harmonic analysis. The gauge resolution is 60 nm and the range is + or - 1mm in the configuration used in this research.

4.2.2 Form Talysurf 120L

Cross sectional roughness characteristics are measured by a Rank Taylor Hobson form Talysurf 120L using version 4 software. The Talysurf is equipped with a 120mm traverse unit and a laser displacement transducer. This system is capable of acquiring up to 120,000 data points per measurement traverse and has a vertical resolution of 10nm to 37.5 nm depending on the desired range. In this investigation a type 112/1836 stylus was used which results in a range of 6 mm, resolution of 10 nm, and has a standard conisphere type diamond with a tip radius of 2 μm. The force applied to the sample by

the stylus is between 0.7 and 1 mN.

Parameters which are referred to in this investigation are defined as follows: Surface roughness is characterized by three parameters. The first is Ra, which is average roughness, and is defined by

$$Ra=\frac{1}{L}\int_0^L \mid z(x) \mid dx.$$

where L is the length of data taken and z is the height above, or below, the average height taken during the sample at position x.

The second roughness parameter is RMS roughness, Rq is defined as

$$Rq=RMS=\sqrt{\frac{1}{L}\int_0^L \mid z^2(x) \mid dx}.$$

The third roughness parameter referenced is Rt, which is total roughness, or peak to valley roughness. This is simply the difference between the highest and lowest points about the mean line.

Kurtosis, R_{ku}, describes the shape or sharpness of the amplitude distribution curve. It is defined as

$$R_{ku}=\frac{1}{lRq^4}\int_0^l Z^4(x)\,dx.$$

Skewness, R_{sk}, describes the symmetry of the amplitude distribution curve about the mean line. Skewness is defined as

4.2.3 ZYGO Laser Interference Microscope

$$R_{sk}=\frac{1}{lRq^3}\int_0^L Z^3(x)\,dx.$$

The ZYGO laser interferometric microscope is a non-contacting roughness measuring instrument which uses computerized phase measuring interferometry to achieve sub-nanometer vertical resolution. The ZYGO is capable of acquiring surface data over an area ranging from 70 μm to 7 mm square with sampling intervals ranging from 27.0 μm down to 0.27 μm. Samples with reflectivities ranging from less than 1% up to 100% may be analyzed both quantitatively and qualitatively using this instrument. The instrument also reports P-V, rms, Ra, Rp, Rv, Rsk (skew), Rku (kurtosis), H (Swedish Heights), Tp (bearing ratio), Xsag, Ysag, radius of curvature, twist, angle, tilt, autocovarience, power spectrum, and a histogram of surface heights for the data taken.

The results given by the ZYGO are comparable, but not the same, to those given by the Talysurf instrument. One must keep the differences in mind when interpreting data taken by the instrumentation. The ZYGO gives values based on a three dimensional data, where the Talysurf data is only measures one line of data and represents only two dimensions. The ZYGO therefore usually gives higher values when measuring P-V, since the instrument covers a larger area (assuming the same overall "trace" length). The ZYGO can also distinguish a 'scratch' from a 'pit' on the surface of a sample, which without additional hardware and software, the Talysurf can not distinguish.

In most of the measurements given in this report, the Talysurf was used to measure the surface properties. This was done for two reasons: 1) the Talysurf can acquire and process data slightly faster than the ZYGO, and 2) the Talysurf can measure rougher profiles than the ZYGO. Until the surface roughness of the samples reach below

approximately 75μm Ra, the ZYGO was not able to consistently acquire data.

4.3 Experimental Procedure

Before an experiment is performed, the 1/2" (12.5 mm) diameter, as received, ground stainless steel samples are measured using the Talyrond and/or the Talysurf, depending on what is being studied. The rod may also be weighed if mass removal rate is to be calculated. Usually three sets of measurements are taken using the instrumentation, and the results are recorded. Initial roughness of the samples is usually ~0.2 μm Ra, and roundness is ~1 to 2 μm out of round, usually due to an odd number of lobes on the rod as a result of the centerless grinding operation used to grind the rods. Initial mass of the rods is ~150g.

After the rod is characterized it is mounted on the lathe using an adjustable 3 jaw chuck. It is then centered within a few micrometers by adjusting the chuck. To measure the eccentricity, a Pneumo-Centric LVDT transducer measures the displacement of the rod while the chuck is rotated by hand.

Once the sample is centered on the lathe, abrasives are added to the magnetic poles, type and quantity depending on the specific test. The abrasive powder forms an abrasive brush as shown in Figure 4.3.1. The rod is then rotated slowly and the magnetic poles are moved until the magnetic abrasives form a brush over the workpiece. The slow rotation helps the rod displace the abrasive brush when the rod is inserted into the brush. When the abrasives cover the sample in the desired location the magnetic field strength (or coil current) is set to the desired magnitude, then the vibration of the magnetic poles and the rotation or the workpiece is started at the same time.

Figure 4.3.1: Photograph of magnetic abrasive brush formed over a stainless steel workpiece. Note that the brush is formed over and under the workpiece since the workpiece is non-ferromagnetic.

During the finishing operation the sample may be removed periodically for roughness, roundness, or mass measurements. Attention should be paid to disturbing the abrasive brush while taking measurements, either not moving the brush, or stirring the brush depending on the experiment. When the abrasive brush is removed from the rod by moving the poles away from the sample in the axial direction, the brush usually remains in the same shape that it has when around the sample. The brush will have a 1/2" hole through the center. Before the sample is removed from the chuck, compressed air is used to blow as much contamination, such as abrasives or lubricant, as possible. The sample is then washed with methanol to remove any remaining residue. The rod is then removed from the chuck and measurements are taken as needed. After the measurements the rod is recentered and the finishing operation is continued.

Chapter V

Test Results

This chapter describes the results of this investigation. It is divided into three sections. The first is roughness and material removal rate when finishing 303 stainless steel, and the second is roundness when finishing stainless steel. The trends in each during the finishing process are presented, along with the effects of finishing parameters. The third is the results of finishing a silicon nitride rod. The resulting surface finish and roundness are presented.

5.1 Roughness and Material Removal Rate in Finishing Stainless Steel

The primary goal of this research is to produce smooth surfaces on cylindrical non-ferromagnetic work. Smooth being quantified as having a roughness of below 50 nm Ra. This section describes the parameters which have been determined to effect the surface roughness of the sample, such as lubricant, rotational/vibrational speeds, field strength etc. Since material removal rate is also a topic of interest which directly affects the rate of change of roughness, material removal rate is described here in conjunction with surface roughness.

This process was found to be capable of generating smooth surfaces on the order of 10 nm Ra. One such surface is shown in Figure 5.1.1 which is a photograph of an

unfinished and finished stainless steel rod. Given in Figure 5.1.2 is Talysurf traces of unfinished and finished surfaces, illustrating the change in surface roughness obtained by this process.

5.1.1 Trends in roughness during polishing

The starting roughness of the stainless steel samples was ~0.2 μm Ra. From this point, the roughness usually decreases exponentially with time. It is apparent that the function for roughness with respect to time generally follows the following relation:

$$Ra(t) = (Ra_0 - Ra_f)\, e^{-\frac{t}{\tau}} + Ra_0$$

where Ra_0 is the initial roughness of the material, Ra_f is the minimum roughness resulting from the finishing conditions, and τ is a time constant for the process which is usually on the order of a minute. Figure 5.1.1.1 is an example of a roughness versus time curve with roughness plotted on both linear and log scales. It is apparent that the curve plotted on the log scale is linear with respect to time until it achieves the minimum roughness obtained, at which point the roughness is nearly constant.

5.1.2 Lubricant

Dry and liquid lubricants were tested during these series of investigations. Zinc stearate, $Zn[CH_3(CH_2)_{16}COO]_2$ was used as a solid lubricant, and oil, SAE 30 etc., was used as liquid lubricant.

Liquid lubricants were found to result in smooth finishes when bonded type

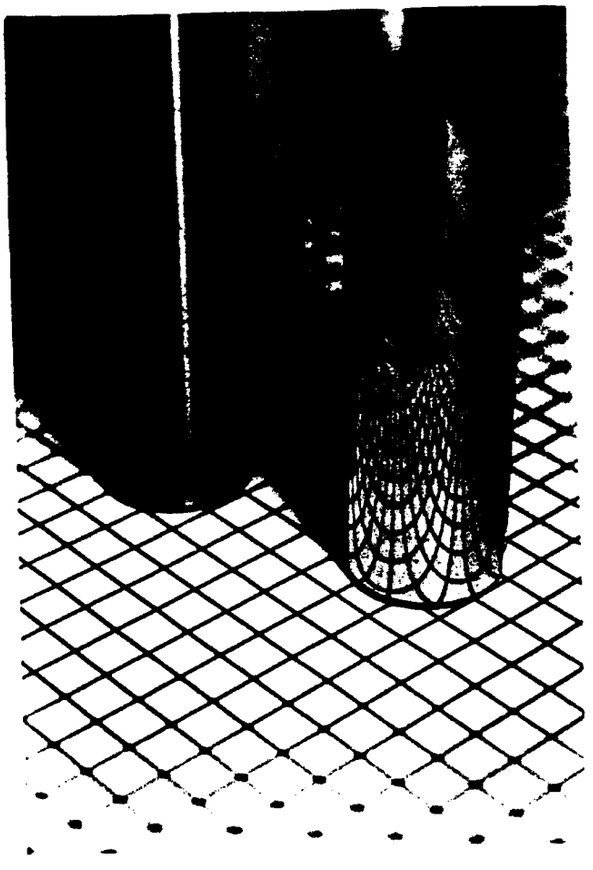

Figure 5.1.1: Unfinished (left) and finished (right) stainless steel rods.

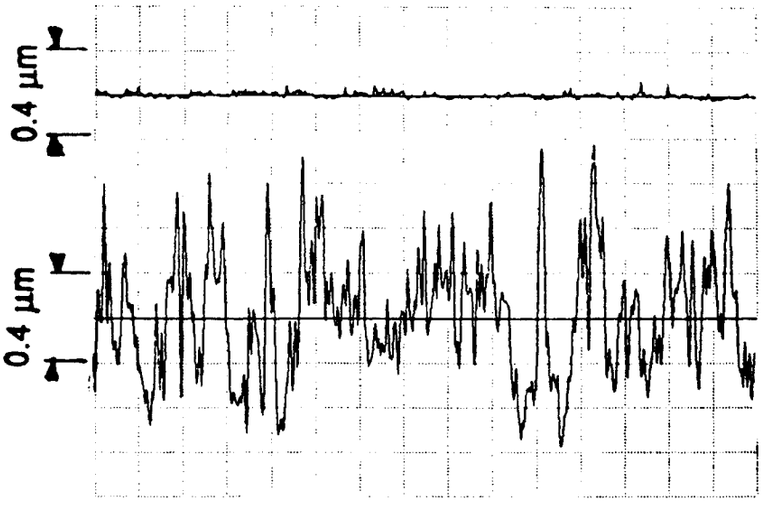

Figure 5.1.2: Talysurf traces of unfinished and finished stainless steel.

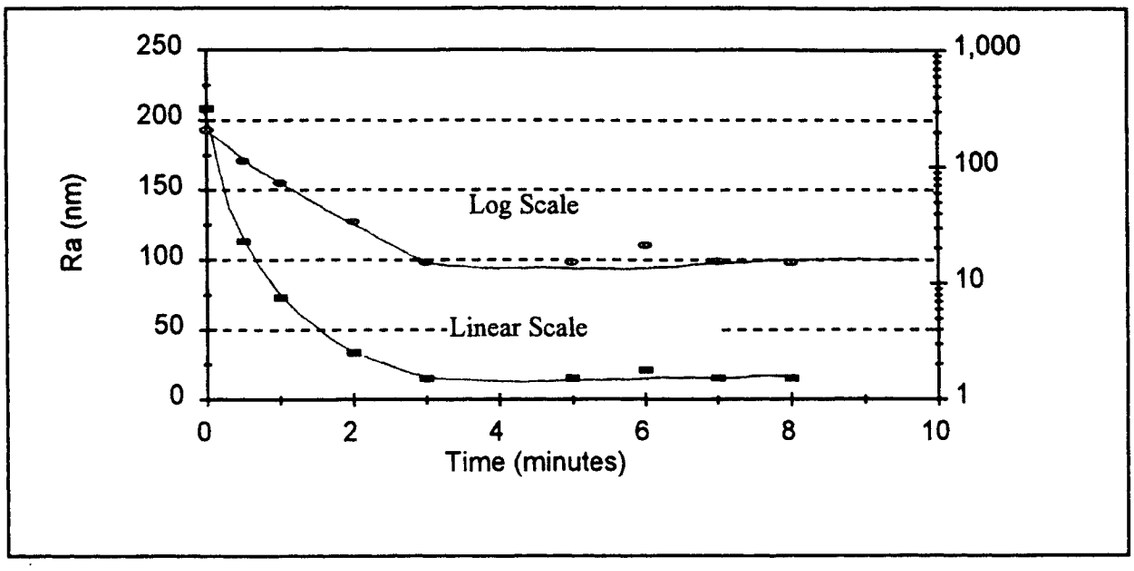

Figure 5.1.1.1: Roughness versus time trend plotted on linear and log scales to show the logarithmic property of the data.

abrasives are used, however when unbonded type abrasives were tested, smooth finishes were not obtained. Figure 5.1.2.1 compares surface finish and material removal rate of bonded and unbonded type abrasives. It is shown that both samples began with a surface roughness around 200 nm Ra. Unbonded abrasives resulted in a relatively high material removal rate with respect to that of the bonded type abrasives. Surface finish resulting from the bonded type abrasives improved to around 25 nm Ra while the surface of the sample finished with the unbonded abrasive became rougher, and reached 300 nm Ra. While finishing with the unbonded type abrasives, the abrasive particles could be heard stirring. For this reason, 3 body abrasion was suspected as opposed to the predominately 2 body abrasion resulting from bonded type abrasives.

The sample polished using the unbonded type abrasive was examined using a scanning electron microscope (SEM). Figure 5.1.2.2a is a micrograph of the resulting surface. Note that scratches are not present on the surface of the sample, which may indicate that 3-body abrasion is occurring. To determine if the resulting surface damage was a result of the silicon carbide particles, a sample was finished using the same conditions as before (given in Figure 5.1.2.1) using unbonded type abrasives, however the silicon carbide particles were not added to the abrasive mixture. The abrasive mixture only consisted of 40# iron. A micrograph of the resulting surface is given in Figure 5.1.2.2b. Notice that the surface morphology is primarily a result of cutting or ploughing (2-body abrasion modes), and "pits" which may result from 3 body abrasion are not present. It is, therefore, proposed that when unbonded type abrasives are used in conjunction with liquid lubricant, the loose abrasive particles remove material from the workpiece by three body abrasion, which under the conditions used in this investigation

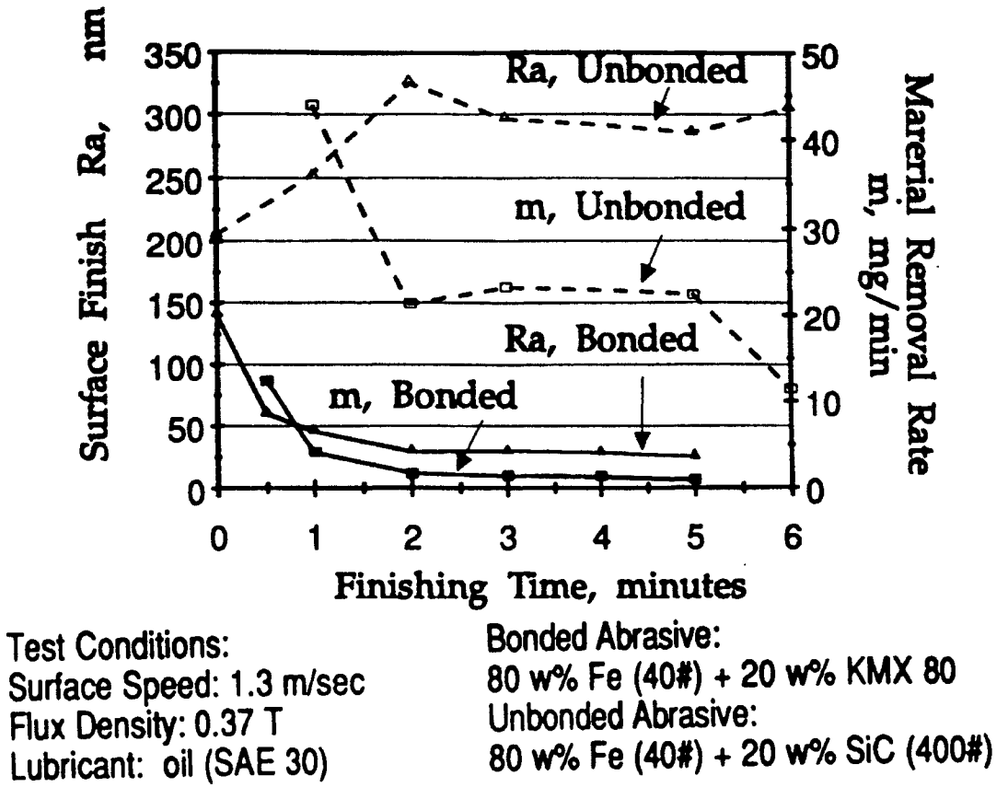

Figure 5.1.2.1: Variation of the surface finish (Ra) and material removal rate with finishing time for bonded and unbonded magnetic abrasive.

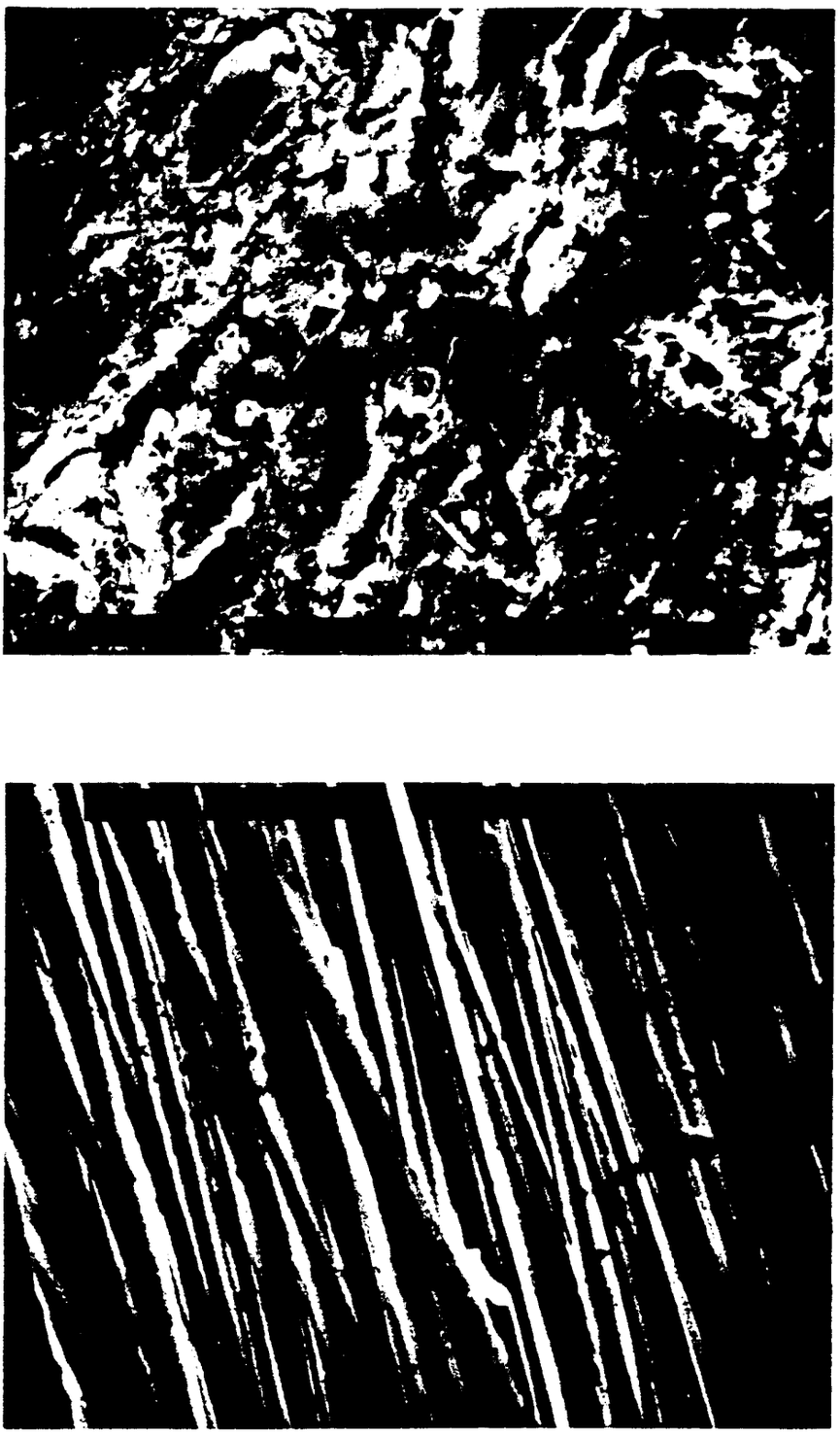

Figure 5.1.2.2: a)micrograph of stainless steel sample polished using unbonded mixture on iron (40#) and SiC (400#) with oil lubricant. b) without SiC.

do not result in improved surface finish.

The first experiment using solid lubricants, explores the effects of the amount of zinc stearate on the finishing performance. For this test, KMX 80 type abrasive was used with an applied field strength of 0.37T. The surface speed due to rotation was 1.3 m/s. Four data points were taken with the amount of zinc stearate varying from 0 to 8 weight percent relative to the abrasive weight. Each test was ran for a total of 5 minutes. The resulting surface finishes after polishing are plotted in Figure 5.1.2.3.

The tests indicate that without zinc stearate, the roughness decreased to around 100 nm Ra after 5 minutes. With 4 to 6 %, the surface roughness was significantly lower, reaching below 30 nm Ra. With excessive amounts of lubricant, the finishing process was slowed, and the roughness only lowered to around 120 nm Ra. From these data, it is evident that the zinc stearate content of the abrasive mixture should be above 3 wt. % and below 6 w/o for minimum roughness to be achieved with respect to time, under these finishing conditions..

5.1.3 Effect of stirring abrasive mixture

During the finishing process, there is very little, if any, stirring, mixing, etc. of the abrasives forming the brush when a solid lubricant is used. Therefore if the sample is removed for in-process measurements, the abrasives may be disturbed, and, therefore, the results of the experiment will be affected. During initial experiments, this phenomena was observed. When the sample was removed in intervals of, say, 1, 2, 4, and 8 minutes, the results indicate that the material removal rate decreases with respect to time, which, perhaps, may be expected due to material being harder to remove as the sample becomes

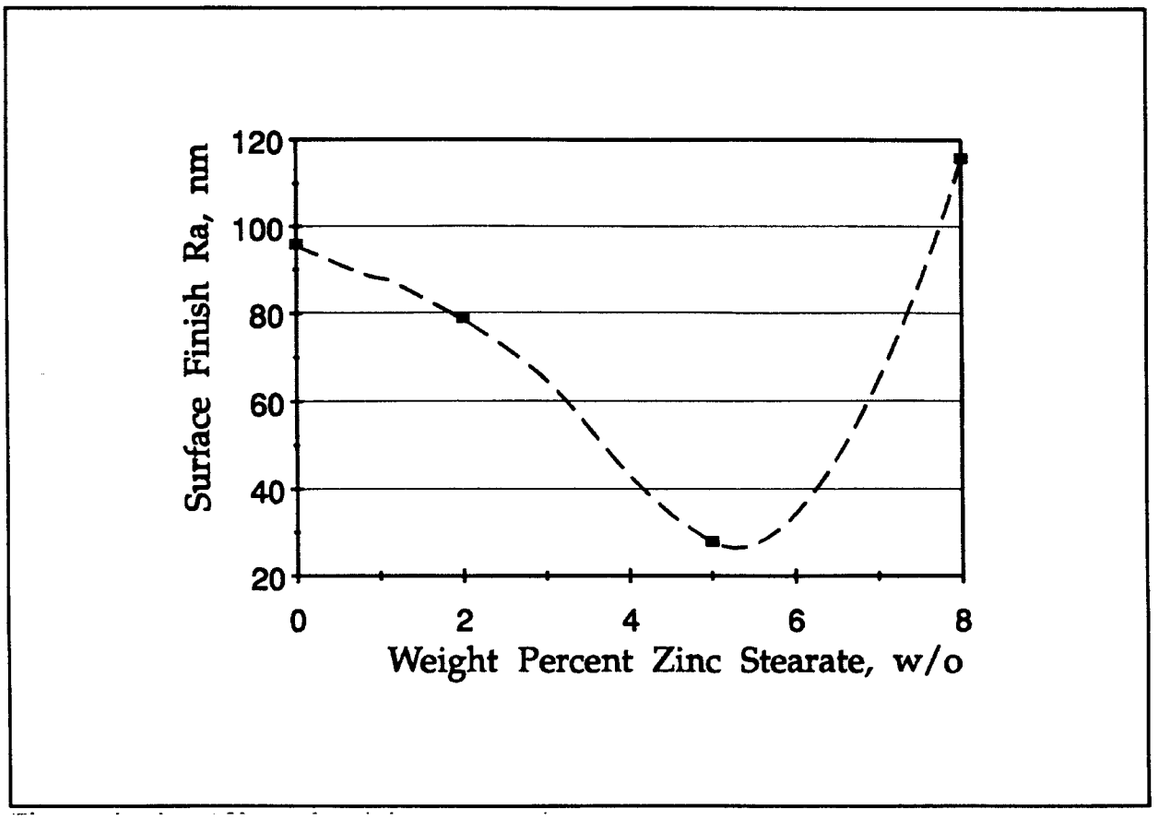

Figure 5.1.2.3: Effect of weight percent zinc stearate in abrasive mixtures on surface finish after 5 minutes. (see text for conditions)

more smooth. However if during the polishing process, measurements are taken at say, 1, 2, 4, 8, 9, and 10 minutes, the material removal rate was found to increase between the times of 8 and 9, and 9 an 10 minutes, with respect to the time between 4 and 8 minutes which is a result which is not supported by the previous argument of material being harder to remove due to the workpiece becoming smooth.

Data were compiled to determine the effect of stirring the abrasives had on the finishing process during measurements under the same experimental conditions., the results are plotted in Figure 5.1.3.1. One curve is a plot of surface roughness versus finishing time when the abrasive brush is disturbed as little as possible while measurements are taken, this data is labeled "stirred". The second set of data is a result of stirring the abrasive brush, by hand, every minute. The results indicate that the material removal rate in the case of the stirred abrasive is higher than that of the unstirred. The surface roughness of the 'stirred bar' also decreased faster than that of the 'unsturred bar', the stirred reaching around 25 nm Ra in only 2 minutes while the unstirred took 7 to 10 minutes to reach the same surface roughness.

There are several possibilities for stirring of the abrasives to influence the finishing process, two of which are described here. The first is that the abrasive particles may become "clogged" with the material removed from the work, and the second is that the abrasive particles may become "dull" and reduce their ability to cut. Figure 5.1.3.2 is a micrograph of one of the abrasives which was used to finish stainless steel. The smooth tip is a result of stainless steel packing in the abrasive. In either case, stirring of the abrasives exposes fresh abrasives to the finishing area periodically, which increases the material removal rate.

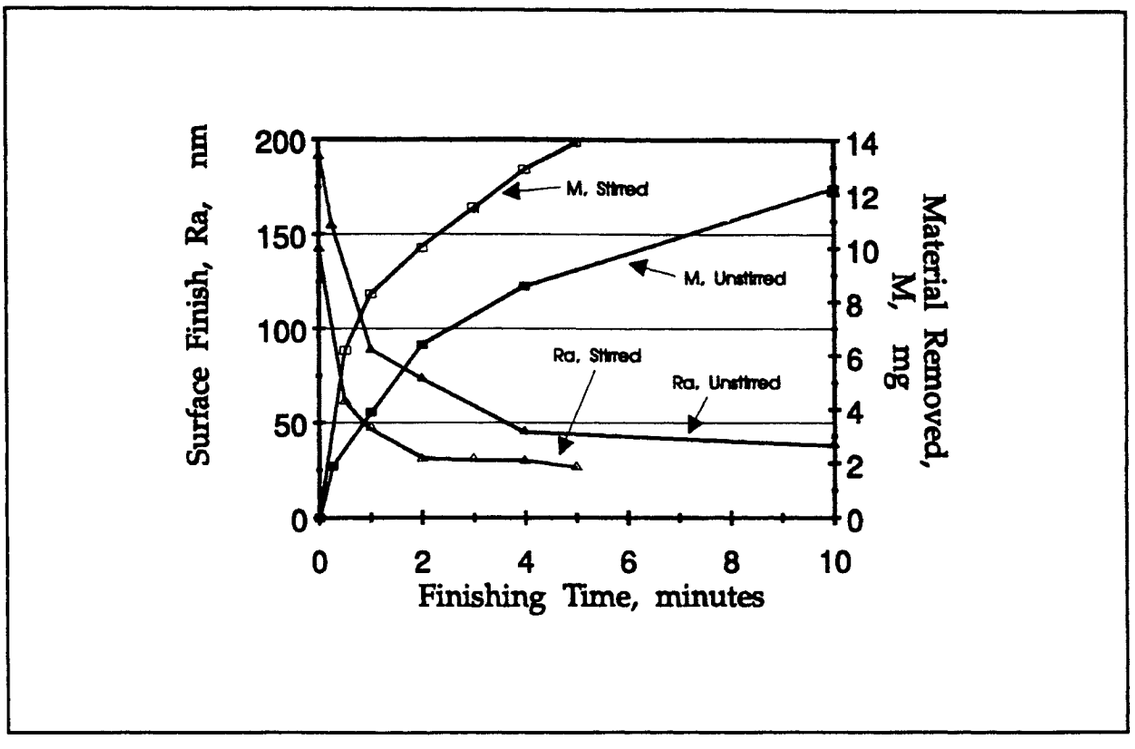

Figure 5.1.3.1: Roughness and material removal versus finishing time curves for stirred and unstirred abrasives (see text for other conditions)

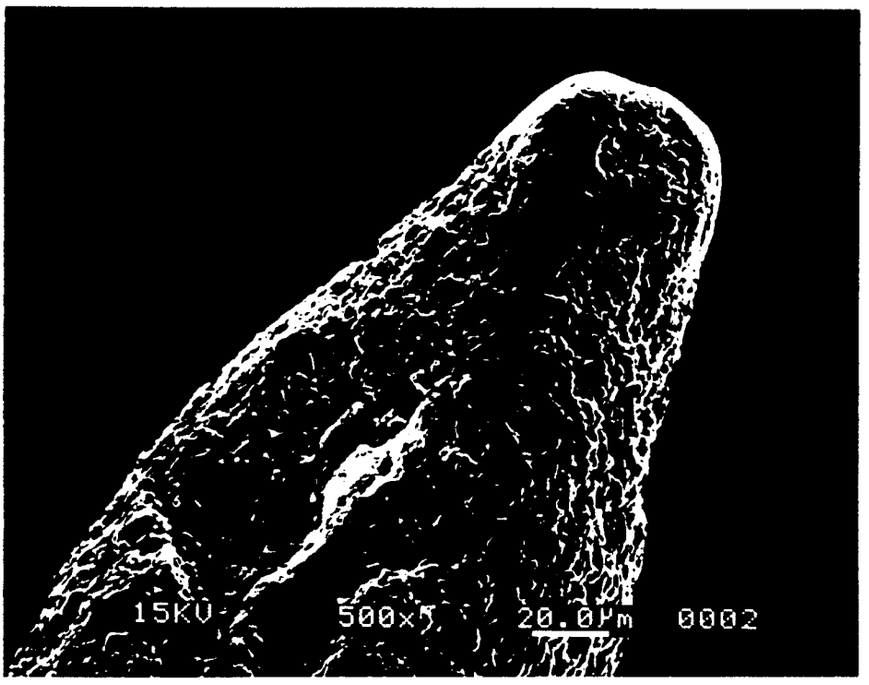

Figure 5.1.3.2: Spent magnetic abrasive used to finish stainless steel.

5.1.4 Vibration and Rotational Velocity

The removal rate, in the case of stainless steel, is not only a function of relative speed between the workpiece and the abrasive, but is also a function of the direction of the velocity. Since the direction is determined by two components, rotational component and vibrational component, when the relative magnitude of each is changed, the removal rate is affected.

Figure 5.1.4.1 is a graph of material removal rates as a function of rotational speed and vibrational speed. It is evident from this graph that there is an optimum combination of rotation and vibration which results in the highest material removal rate. In the case of these polishing conditions it appears that the optimal rotational speed is around 500 rpm.

By calculating the linear velocity of the two velocity components, an included angle, θ_h, may be defined as illustrated by Figure 5.1.4.2. It may be calculated from

$$\theta_h = \tan^{-1}\left(\frac{V_{vmax}}{V_r}\right)$$

where V_{vmax} is the maximum velocity resulting from vibration, and V_r is the velocity resulting from rotation of the workpiece. V_{vmax} can be determined by assuming that the

Workpiece:	11mm Dia. Hot Pressed Silicon Nitride Bar
Abrasive:	400μFe + 1μ Cr_2O_3 (Unbonded type)
Rotational Speed:	3000 rpm
Pole Vibration Frequency:	20 Hz.
Magnetic Flux Density:	0.6 T
Finishing Time:	15 Minutes

Table 5.3.1: Conditions used for finishing silicon nitride rollers by MAF.

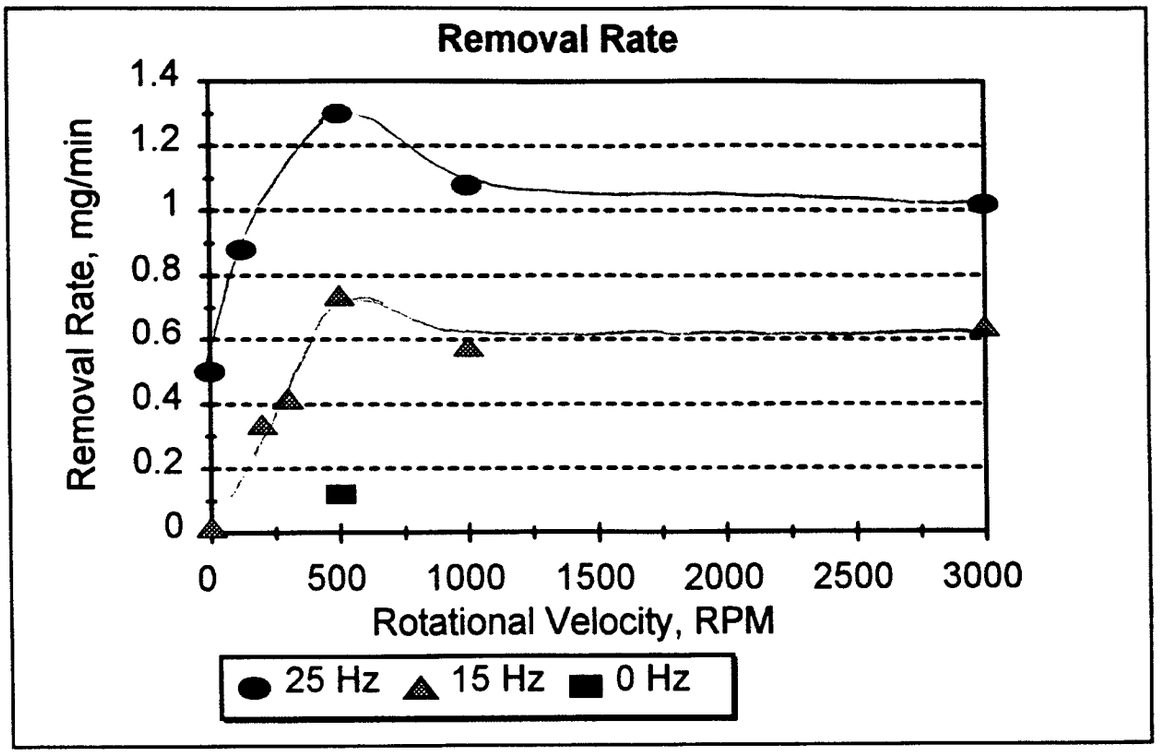

Figure 5.1.4.1: Mass removal rate as a function of workpiece rotational speed and magnetic pole vibration frequency.

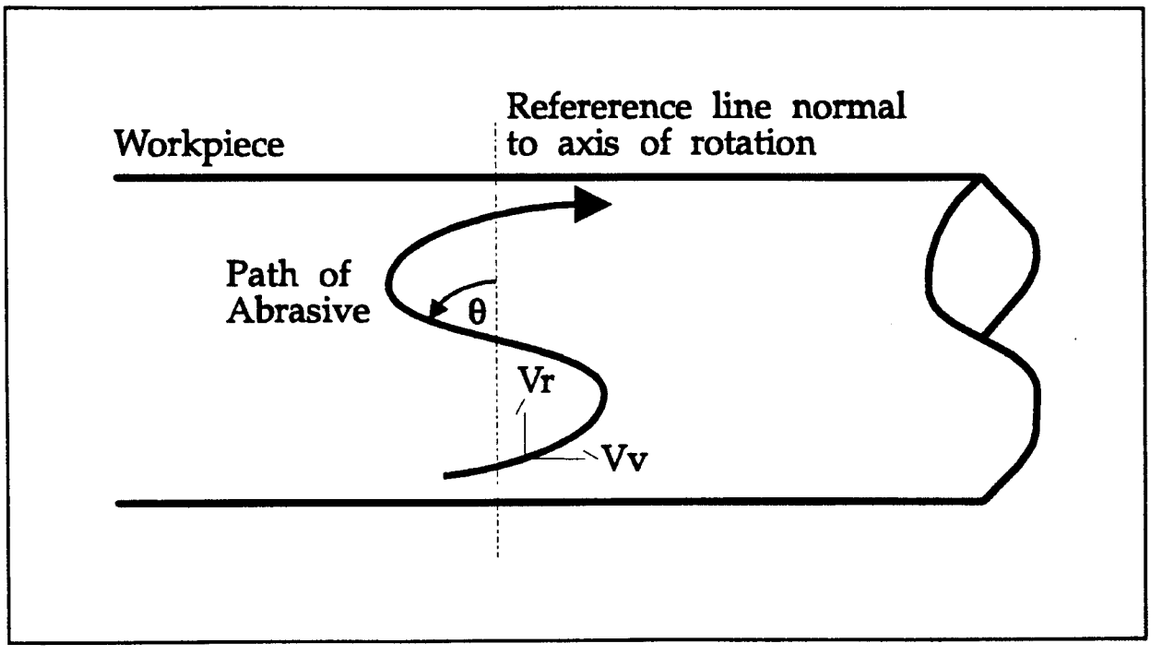

Figure 5.1.4.2: Abrasive path resulting from rotational and vibrational velocity components. half included angle is labeled θ.

oscillation is of the form x = (A/2) sin(ω t) where ω is the frequency of vibration (rad/s) and A is the amplitude of vibration. The velocity can then be calculated by the derivative as v = (A/2) ωcos(ω t). The maximum velocity which is the V_{vmax} value desired, can be determined by forcing the cosine term to unity. The result is

$$V_{vmax} = \frac{A\omega}{2} = \frac{A(2\pi f)}{2} = \pi A f$$

where f is the vibrational frequency in Hz. The calculation for V_r is simply

$$V_r = \frac{D}{2}\omega = \frac{D}{2}\frac{(2\pi\Omega)}{60} = \frac{\pi D\Omega}{60}$$

where D is the diameter of the workpiece, ω is the rotational speed in rad/sec, and Ω is the rotational speed in rpm.

A graph of half included angle as a function of workpiece rotational speed and vibration frequency is given in Figure 5.1.4.3 for the conditions used in this experiment. The ranges given in the graph are roughly the ranges which may be achieved by the existing experimental setup. This plot enables one to establish what angles are possible and the conditions in which the angles may be achieved.

The effect of half included angle, θ, on material removal rate is shown in Figure 5.1.4.4. This graph shows the effect that half included angle and vibration frequency have on material removal rate. The results of this plot indicate that the half included angle which results in the highest material removal rate, is somewhere around 30 to 40 degrees.

Another interesting result is obtained when material removal rate per sliding

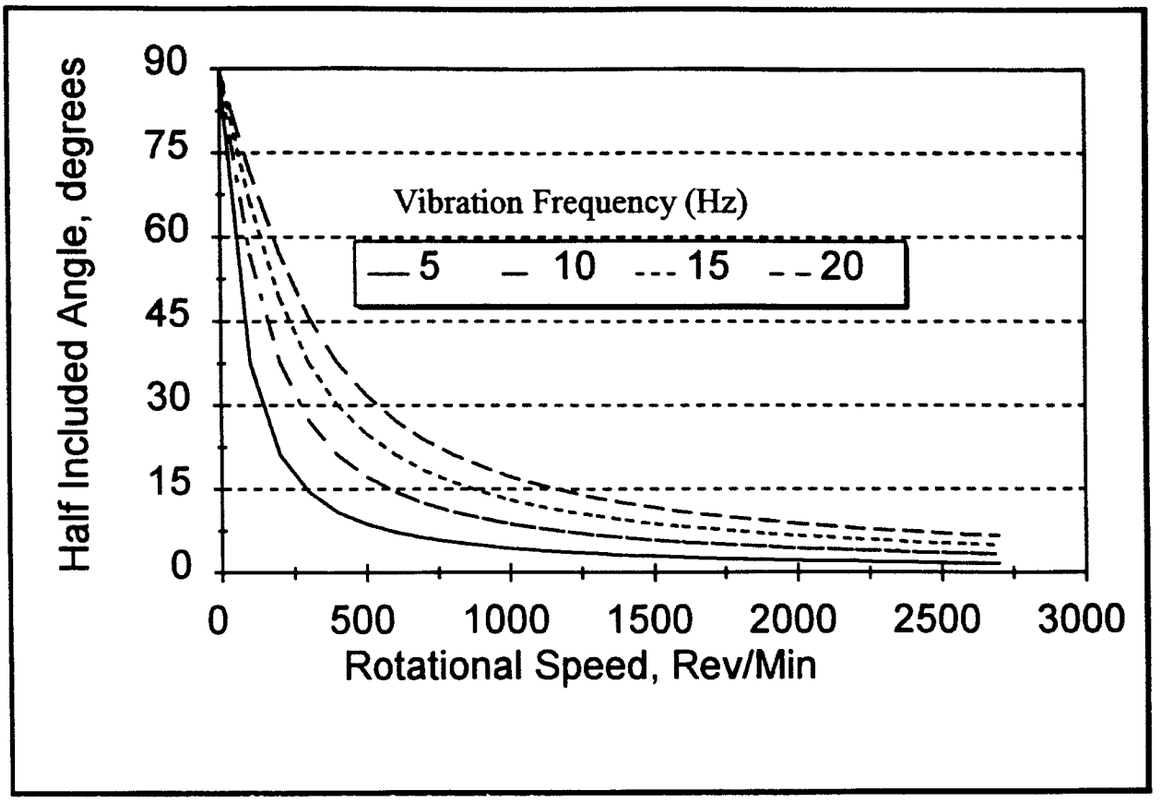

Figure 5.1.4.3: Half included angle as a function of workpiece rotational speed and pole vibration frequency for given conditions.

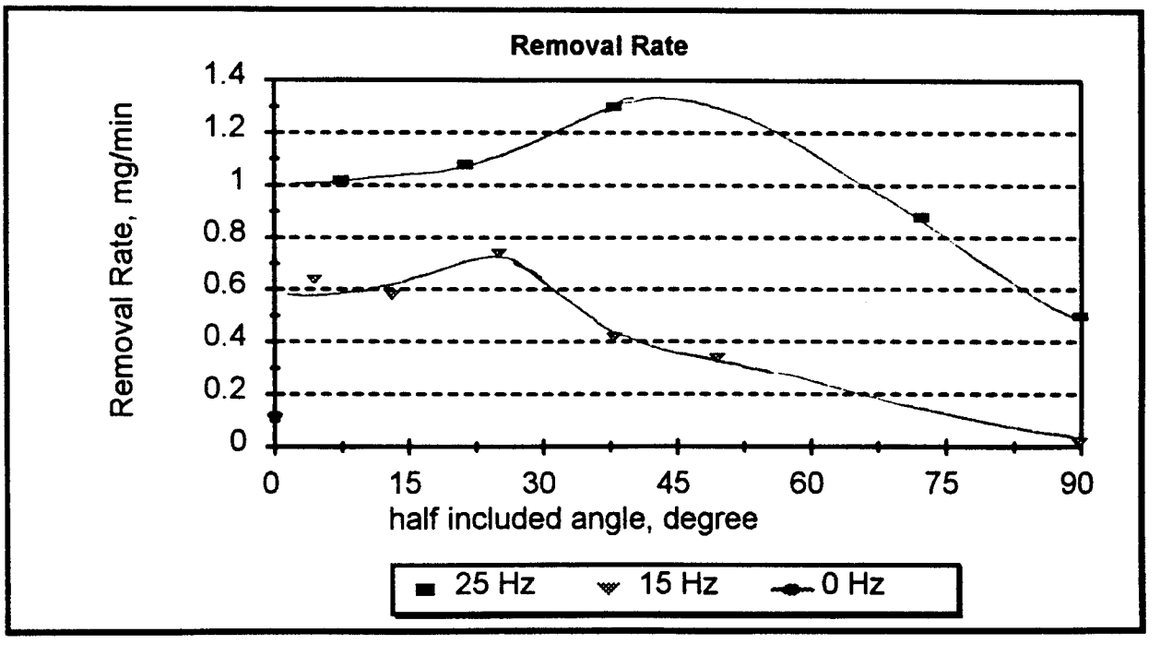

Figure 5.1.4.4: Effect of half included angle on material removal rate.

distance is plotted against half included angle, as in Figure 5.1.4.5. These data indicate that the maximum material removal per sliding distance is achieved at half included angles around 50 to 60 degrees, which is a larger angle than that which resulted in the maximum material removal rate.

Since it appears that the direction of the scratches produced on the surface of the workpiece may have a significant influence on the material removal rate per sliding distance, an RMS value may be more representative of the mean scratch angle on the surface of the workpiece. Therefore, the material removal rate is plotted as a function of the RMS half included angle, which is simply 0.707 times the half included angle since sinusoidal oscillation was assumed. It can be seen in this plot that the maximum material removal per sliding distance is around half angles of 45 to 50 degrees.

Material removal rate is not the only result that must be investigated under these conditions. Resulting surface roughness is also of interest. If surface roughness after the experiment is plotted against half included angle, as in Figure 5.1.4.7, the result indicates that the minimum roughness at this given time results when the half included angle is around 20 to 30 degrees. This result is in the same range of half included angle which results in the highest material removal rate with respect to time.

5.1.5 Effect of coil current

An increase in current in the magnetic coil results in higher magnetic flux density in the working zone, which in turn results in higher finishing pressures. Therefore, finishing pressure increases with an increase in coil current. This can be seen by plotting the force on half of the magnetic brush as a function of coil current as shown in Figure 5.1.5.1.

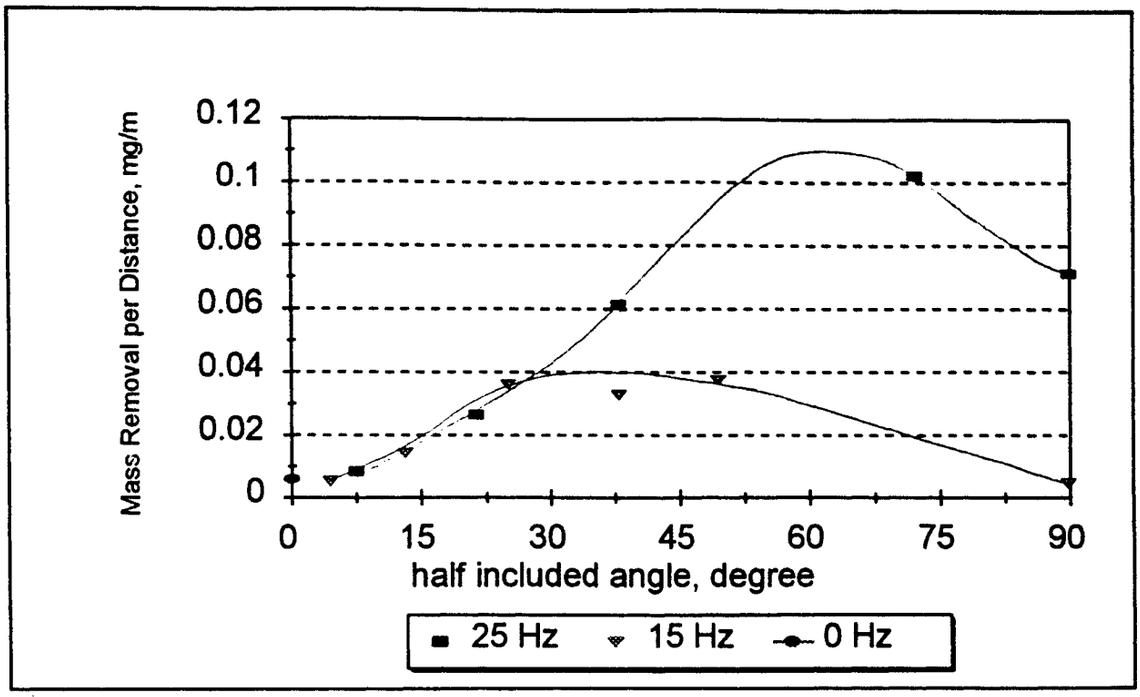

Figure 5.1.4.5: Effect of half included angle on material removal per sliding distance.

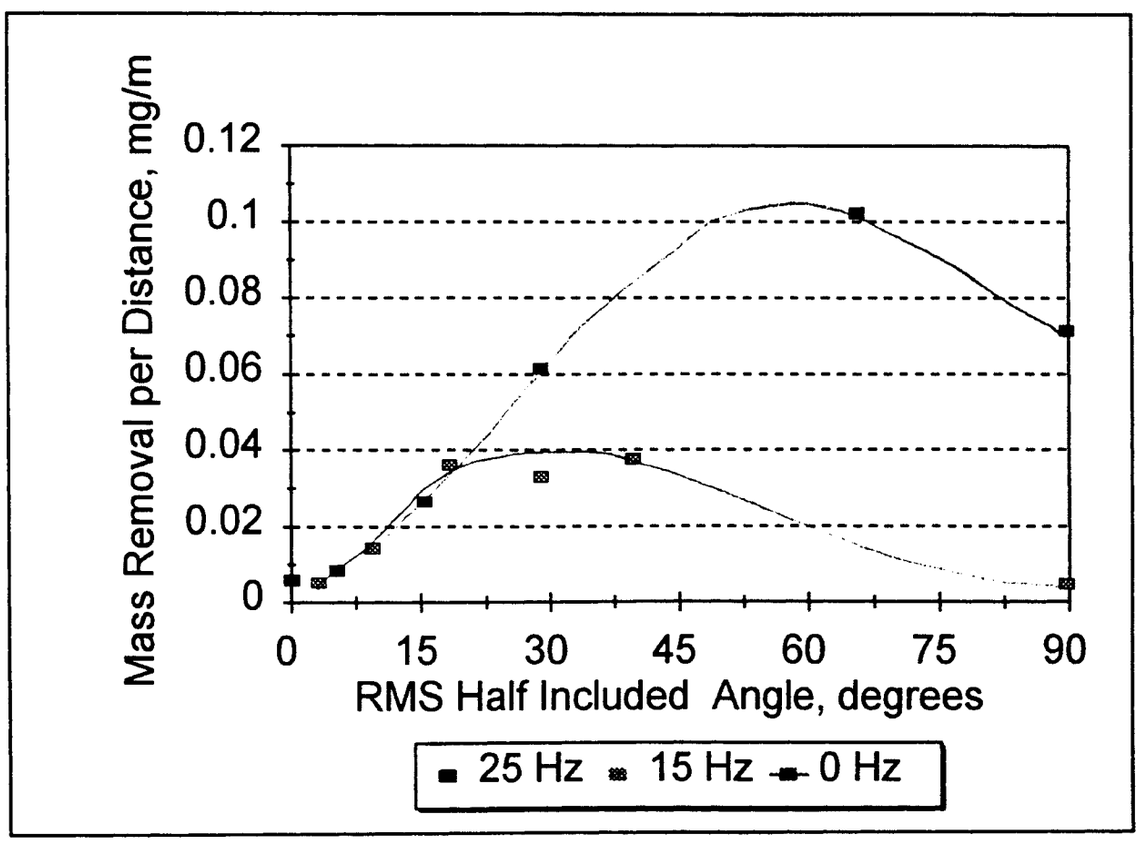

Figure 5.1.4.6: Effect of RMS half included angle on material removal per sliding distance.

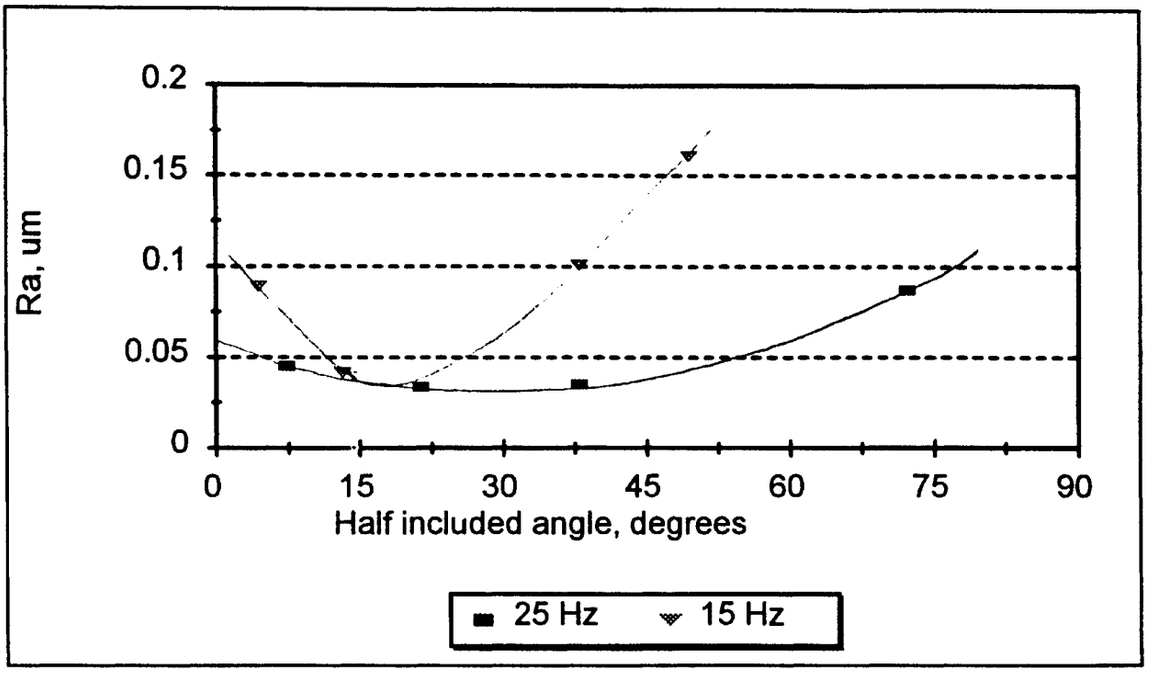

Figure 5.1.4.7: Surface roughness (Ra) as a function of half included angle after 5 min. finishing time.

The data in Figure 5.1.5.1 were obtained by using a nonrotating thin brass tube as a workpiece, which is equipped with a strain gauge to measure the strain in the tube resulting from bending. An abrasive brush is then formed on the top of the tube only, which results in slight bending of the bar as the abrasive brush exerts pressure on the top of the tube. The strain of the rod is then recorded, which linearly increases with an increase in force. The magnetic flux density tangential to the surface of the tube is measured using a tesla meter inside the abrasive brush on the top of the tube. The result is the correlation between current, magnetic field strength, and total force on the tube (finishing pressure x area).

The data in Figure 5.1.5.1 indicate that as coil current increases, magnetic flux density increases, and the finishing force (pressure) increases. Vibration also increases the finishing pressure as much as two times.

The following data demonstrate the effect that coil current has on surface finish as a function of time under the following conditions: Abrasive: KMX80, Lubricant: 5wt. % Zinc Stearate, Workpiece Speed: 2000 rpm, Vibration Frequency: 20Hz.

Figure 5.1.5.2 is a graph of surface finish versus time, with coil currents of 1 and 2 amps. These data were obtained by fitting the equation given in Section 5.1.1 to the acquired data to get a smooth curve. It is evident that the rate of decrease in surface roughness increases as the current is increased. The finished produced by higher currents also appears to be more smooth than that produced by low coil currents.

5.2 Roundness of Stainless Steel

The general trend for the roundness of a rod during this type of finishing operation

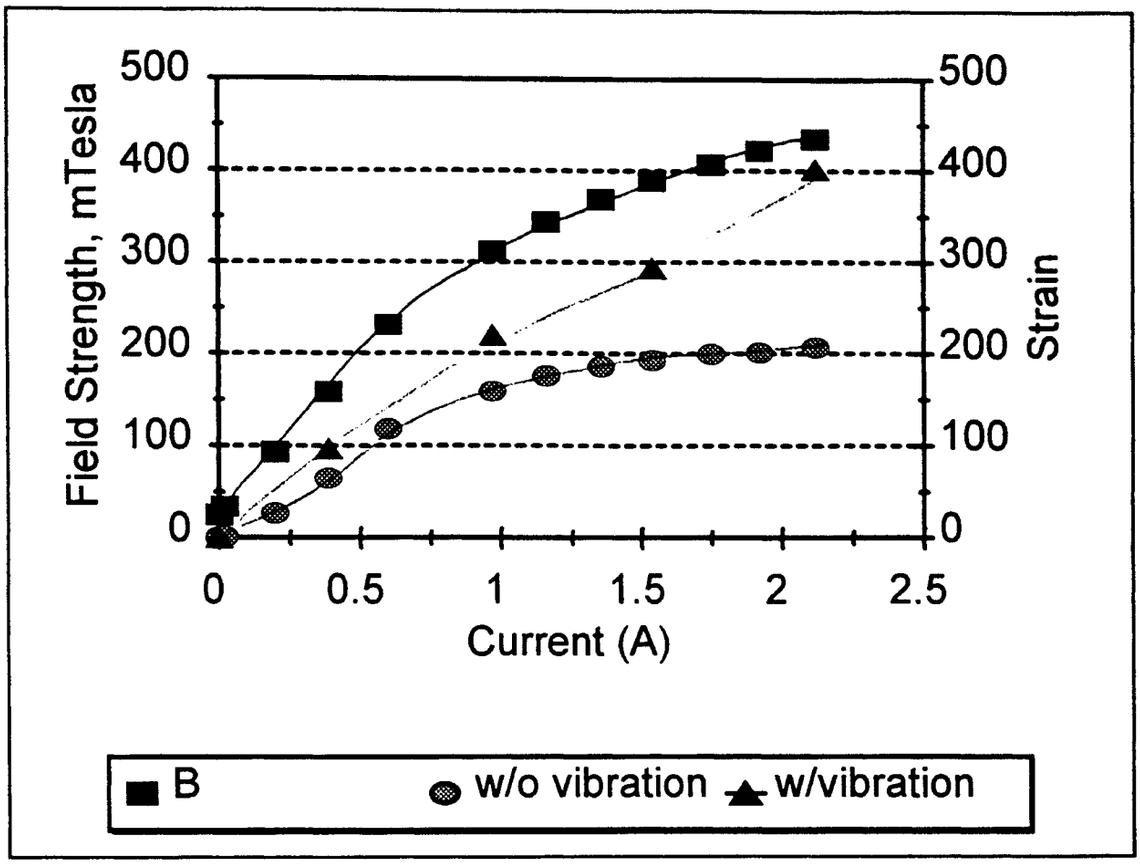

Figure 5.1.5.1: Trends in magnetic flux density and finishing force, as indicated by strain, as a function of coil current.

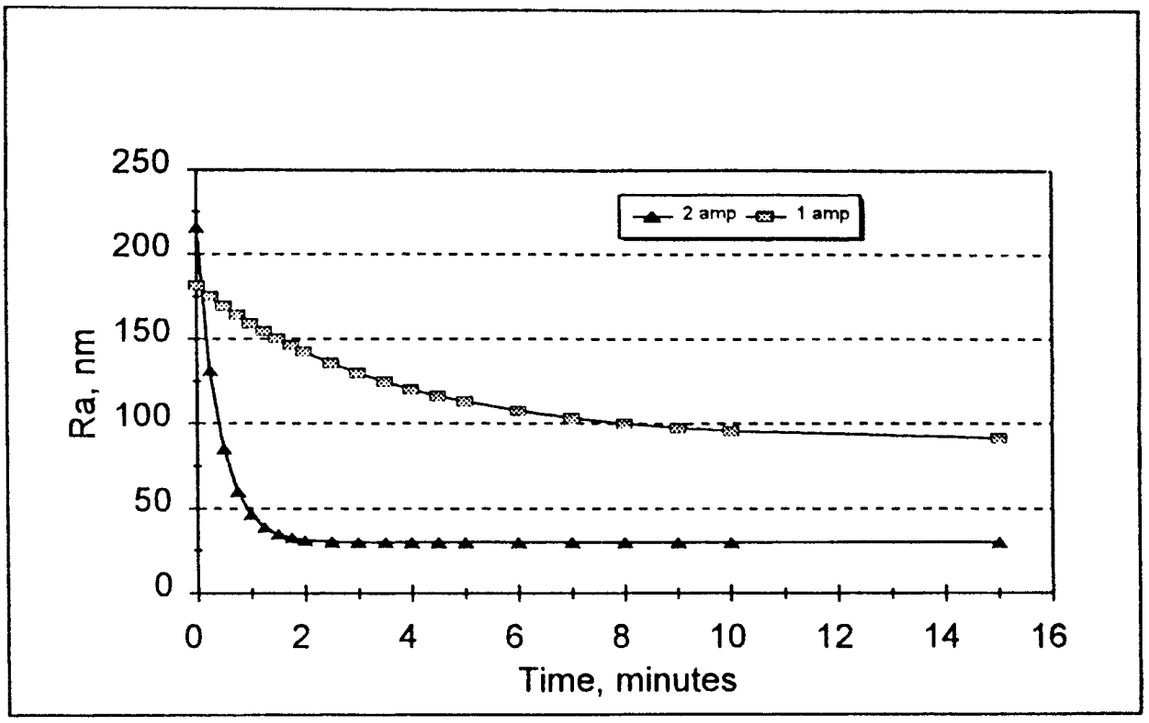

Figure 5.1.5.2: Effect of coil current on surface finish. (see text for finishing conditions)

is for the cylindricity to improve with time. Unlike in centerless grinding which does not have a defined center of rotation and results in a rod of constant diameter with lobes, MAF process has a defined center of rotation and does not result in lobes.

Figure 5.2.1 shows the variation in roundness with respect to finishing time in MAF. The roundness begins at 2.2μm out of round and decreases sharply for the first 30 seconds, then begins a slow decrease in magnitude with a slope of 0.05μm/min. This results in a roundness of 0.9μm out of round after 5 minutes of finishing.

5.3.1 Finishing of Silicon Nitride

A limited number of silicon nitride samples were finished using the MAF technique described in this thesis to establish the suitability of this method for finishing advanced ceramics. The conditions used to finish the silicon nitride sample are given in Table 5.3.1. The abrasives were prepared by mixing approximately 50 volume percent iron with 1μm Chrome Oxide. The mixture was then covered with methanol and stirred until the methanol evaporated. This procedure "unclumped" the chrome oxide powder and left it mixed with the iron powder and appeared to have coated the iron with the chrome oxide. The coating process was evident due to the larger, relative to chrome oxide, iron particles appearing to be green, which is the color of the chrome oxide.

After 15 minutes finishing time the sample showed improved roughness and roundness, and the sample had a mirror finish in the area polished. The unfinished sample had a roughness of 175.4 nm Ra (1.716 μm Rt). After finishing the surface finish improved to 6.1 nm Ra (44 nm Rt). Figure 5.3.1 shows talysurf traces of the unfinished and finished samples.

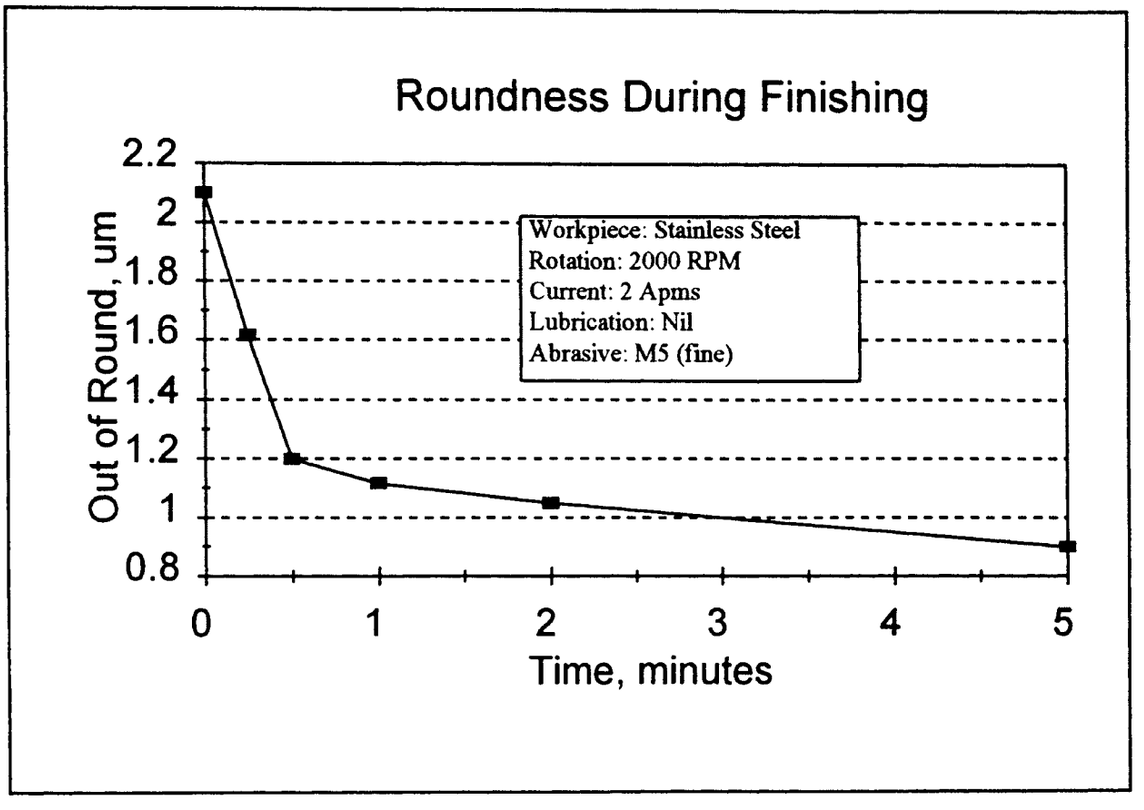

Figure 5.2.1: Variation in roundness with time during MAF.

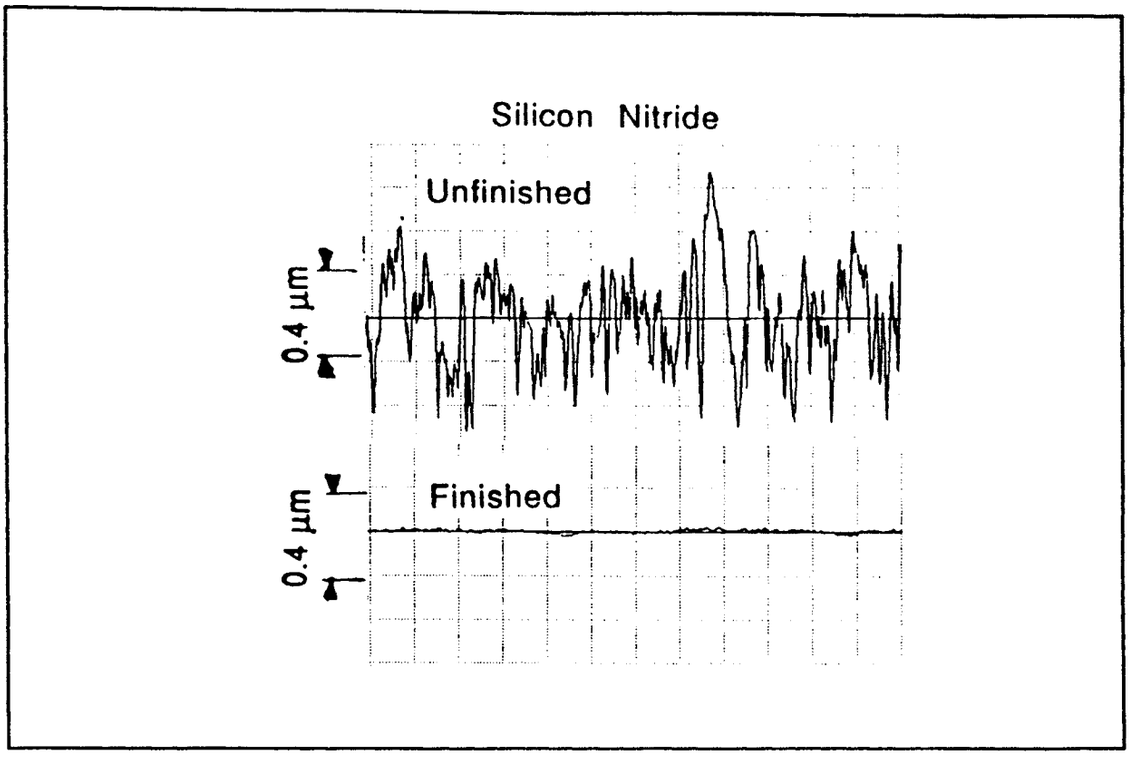

Figure 5.3.1: Talysurf traces of unfinished and finished silicon nitride (conditions given in Table 5.3.1). Unfinished 175 nm, Finished 6 nm.

Roundness of the sample also was improved, the before and after finishing talyrond traces are given in Figure 5.3.2. The initial roundness of the sample was 1.8μm out of round and appeared to have 2 lobes. After finishing the roundness improved to 0.65μm out of round and the lobes were not present.

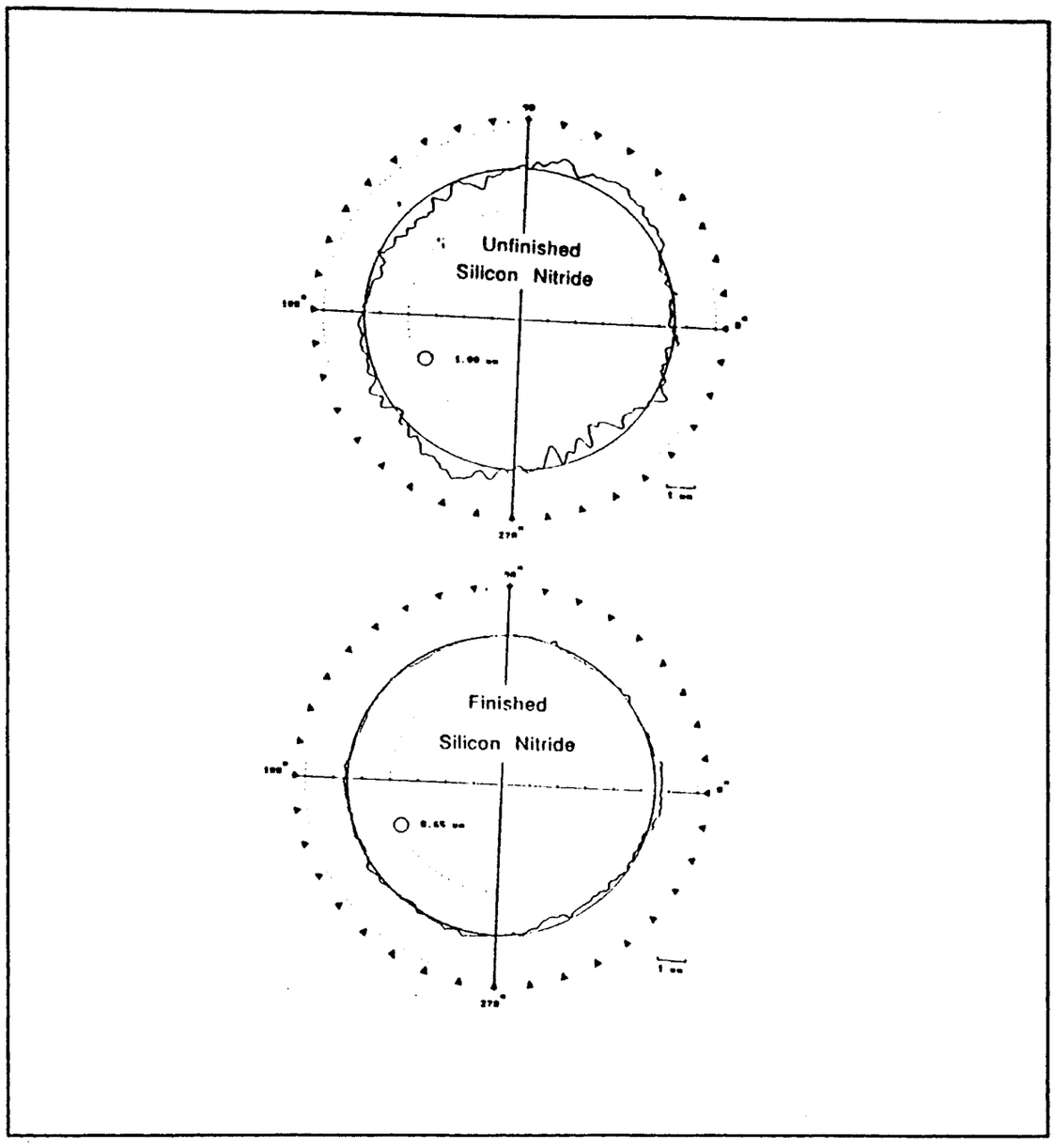

Figure 5.3.2: Roundness plots of silicon nitride before (1.8 μm) and after finishing (0.65 μm).

Chapter VI

Discussion

It was shown in this thesis that MAF can be used to produce fine finishes (Ra < 10 nm) on non-ferromagnetic materials such as stainless steel and silicon nitride cylinders. The later are to be used as rolling elements for bearings. Roughness values ~10nm Ra can be achieved on stainless steel, and around 5 nm Ra on hot pressed silicon nitride using the conditions in this investigation.

6.1 Finishing Non-ferromagnetic Stainless Steel

Based on the experimental results obtained in this investigation, roughness trends as a function of time appears to follow the relationship

$$Ra(t) = (Ra_0 - Ra_f)\, e^{-\frac{t}{\tau}} + Ra_f$$

as mentioned in Section 5.1.1. This trend was first noticed by plotting roughness as a function of time with a log Ra axis. The result was a graph as shown in Figure 5.1.1. which shows an exponential decrease in roughness until a minimum, Ra_f, is reached. Knowing the parameters in this equation may prove to be very useful. For example if the τ and Ra_f values are known, then calculation of the finishing time of a rod with any value of Ra_o is trivial. Or if all parameters are known, and a finish with a magnitude greater

than Ra_f is desired, the finishing time may be calculated to leave the desired surface finish on the rod. The effects on various parameters on τ and Ra_f may be investigated in the future, making the constants in this equation valuable performance indices.

Zinc stearate proved to be a useful solid lubricant, as shown in Section 5.1.2. It was found that little (less than 1 wt. %) or no lubricant, resulted in low material removal rates when compared to rates resulting from around 5 wt. %. Material removal rates then dropped with an increase in zinc strearate above 5%. The increase in removal rates from 0 to 5% may be attributed to lubrication in the abrasive cutting zone, or possibly lubrication of the abrasive powder forming the abrasive brush. Lubrication of the brush may make the brush more flexible, thereby increasing the finishing force by not allowing the abrasive particles to wedge themselves into a 'stiff' shape. The decrease in material removal rates above 5% zinc stearate is attributed to excessive lubrication in the working zone, which impedes polishing action.

During finishing, the magnetic abrasive brush is somewhat rigid, and the abrasive particles are not free to circulate. This sometimes may result in several problems. The first problem is perhaps the most obvious. If the abrasives do not circulate, the abrasives which are in contact with the workpiece may become clogged or dull over time. The second problem is stiffening of the abrasive brush. It was found that the abrasive brush sometimes remains in the same shape after the workpiece is removed from the brush, as it is when the workpiece in inside the abrasive brush. This indicates that the abrasives may be wedging against each other to form a rigid, as opposed to a flexible, abrasive brush. If the rigid brush is formed, then pressure between the brush and the work will be reduced, thus hindering the polishing operation. When one of these situations occur,

erratic roughness versus time plots result, and the data no longer fit the equation given in Section 5.1.1. either because the material removal rate is decreased, thus making τ a function of time, or the roughness of the sample may even increase. Either behavior becomes evident from the roughness versus time plots. To correct these problems, the abrasive brush is stirred periodically when the workpiece is removed from the brush. This can be done simply by "crushing" the abrasive bridge formed by the abrasives, or by agitating the brush by hand. Either method appears to keep the material removal rates constant over time.

The material removal rate when finishing stainless steel was found to be dependent on the half included angle of the velocity determined by the relative velocities resulting from the rotation of the workpiece and the vibration of the magnetic heads. The dependence is believed to be due to the mode of material removal, which are predominately ductile modes such as cutting and ploughing. Material removal rate with respect to sliding distance (wt/distance) reaches a maximum value around 50 to 60 degrees. Perhaps a better representation of this angle is the RMS value of the half included angle. Maximum material removal per sliding distance occurs at 45 to 50 degrees RMS. This result indicates that maximum material removal per sliding distance occurs when the velocity of sliding motion is perpendicular to previous scratches produced on the surface. The lay of the created surface is therefore a cross hatched pattern which results in high material removal.

Material removal per sliding distance is not the only material removal parameter of interest. Also of interest is the material removal rate with respect to time. Maximum material removal rates are achieved at half included angles around 30 to 40 degrees,

which is considerably lower than that which gave maximum removal per distance. This decrease in angle may be explained by noting that the angle may be decreased, by increasing the rotational speed of the workpiece. This increases the rate of sliding with respect to time. Although material removal per distance decreases when the half included angle is decreased, sliding distance increases which compensates for the decrease in removal per distance. This results in higher material removal rates at half included angles around 35 degrees.

Coil current during finishing had some interesting effects on the finishing process. The first in the increase in material removal rate with an increase in coil current. This result was anticipated due to an increase in the polishing forces which result from the increase in coil current. The second result was not anticipated, which is a decrease in final surface finish with an increase in coil current (thus finishing pressure). The cause of this behavior is not yet known. The results plotted in Figure 5.1.5.2 show these effects.

6.2 Finishing Silicon Nitride

The results achieved by finishing silicon nitride are quite good, especially considering that these results are from of a limited number of tests based on the knowledge of finishing stainless steel, and not ceramics. Roughness of the silicon nitride sample was brought down from 175 nm Ra to 6.1 nm, and roundness was taken from 1.8 μm to 0.65 μm in only 15 minutes (see Section 5.2 for the conditions used).

Chrome oxide was chosen for the abrasive constituent based on the mechano-chemical action discussed earlier, that the abrasive may exhibit on silicon nitride, given

high enough pressures and temperatures. A 1 μm chrome oxide powder was chosen in particular due to its small size (smallest available) and high surface energy compared to larger particles. When the chrome oxide powder was mixed with iron powder, a considerable amount of chrome oxide powder fell from the magnetic abrasive mixture when the abrasive brush was formed in the magnetic field. In an attempt to correct this problem. methanol was added to the mixture of powders, and the mixture was stirred until the methanol evaporated. This appeared to leave the iron particles almost completely coated with chrome oxide. When this mixture was subjected to the magnetic field, the chrome oxide remained in the abrasive brush. Since chrome oxide is non-ferromagnetic, if the chrome oxide was not intimately mixed with the iron particles, then the chrome oxide would fall out of the magnetic brush, leaving only iron.

For these experiments, high temperatures and pressures are desired to maximize the probability and rate of mechano-chemical reactions between the silicon nitride and chrome oxide abrasive. For these reasons, friction between the abrasive brush and the work were to be maximum. Therefore high magnetic field and dry conditions were selected to maximize the frictional force, along with 3000 rpm spindle speed and maximum vibration frequency to generate as much heat as possible.

The experiment was conducted for a total time of 15 minutes. After finishing, the silicon nitride rod was hot to the touch, and was found to have a mirror finish in the finished region.

The sample was measured using the talysurf, and results indicate a roughness of about 6 nm Ra. This roughness is definitely approaching the measurable limit using Talysurf equipment, and the results may be subject to external noise and vibration.

Roundness of the sample was improved from 1.8 μm to 0.6 μm. Initial assumption was that in just 15 minutes finishing time, little if any change in part geometry had occurred. However, out of roundness was decreased by 2/3, and lobes which existed on the unfinished rod were removed.

These results indicate that the MAF process is an excellent alternative to traditional methods of polishing, and is extremely effective when polishing advanced structural ceramics such as silicon nitride.

Chapter VII

Conclusions

1. MAF technique has been developed for polishing non-ferromagnetic materials such as austenitic stainless steel and silicon nitride. This technique is equally applicable for finishing ferromagnetic materials.

2. Equipment for MAF has been designed, built, and tested for polishing non-ferromagnetic stainless steel and silicon nitride rollers. This equipment is simple and was incorporated on a conventional precision lathe.

3. An extensive study was conducted on finishing of stainless steel rods. The effects of various parameters, including magnetic field strength, rotational speed, vibration frequency, and lubricant on material removal rate and surface finish was investigated.

4. Surface finish on non-ferromagnetic stainless steel was improved from ~200nm Ra to ~10 nm Ra by MAF.

5. Surface finish on hot pressed silicon nitride was improved form ~300 nm Ra to 6 nm Ra by MAF in 15 minutes while roundness was also improved.

6. As the equipment for MAF is simple and inexpensive and can be incorporated on conventional machine tools, the capital investment in this technology is low compared to the expense of ultraprecision grinding machines. Hence the technology can be economical and cost effective.

7. Based on the experimental data a simple relationship was developed for surface roughness. It was found that the surface roughness decreased exponentially with respect to time using this process and can be described by a relationship of the form $Ra(t)=(Ra_0-Ra_f)\exp(-t/\tau) + Ra_f$ where τ is on the order of one minute in the case of stainless steel.

9. Axial vibration of the magnetic heads was found to be critical for the finishing by MAF. High material removal rates and best finish were obtained with increase in the axial vibration (frequency and amplitude). Both axial vibration and rotational speed of the workpiece has to be taken into consideration for obtaining the best cross pattern that gives the best finish as well as highest material removal rates. Half included angles between 15 and 35 degrees are found to be optimum for best finish and high removal rates.

10. Material removal rates on the order f 1 mg/min are obtainable by MAF when polishing stainless steel.

11. Zinc stearate is an effective solid lubricant for the MAF process and results in the highest material removal rate when mixed as 5 wt. % of the magnetic abrasive powder.

12. Unbonded type abrasives may provide high material removal rates, while bonded type abrasives result in lower surface roughness.

13. Although stainless steel (non-ferromagnetic) meets the requirements as far as simulation of non-magnetic silicon nitride rollers, there are significant other differences. The first among them is the nature of failure of these materials (plastic deformation is the primary mode in the case of stainless steel while brittle fracture, dislodgement of grains, microcracks, and viscous flow of the glassy phase in the case of silicon nitride). Also, work hardening of the stainless steel during polishing leads to fatigue cracks and removal of flakes of stainless steel material.

Chapter VIII

Future Work

This research has shown great potential for MAF in finishing cylindrical components, such as rolling elements for roller bearings, made from non-ferromagnetic materials. Not only is the process capable of mechanical material removal, such as machining stainless steel with alumina, but is also capable of taking advantage of mechano-chemical material removal when machining silicon nitride. This process creates both smooth, and round components.

MAF offers a low cost finishing process which does not require expensive, machine tools, that is capable of finishing advanced materials which have been very challenging and expensive to finish in the past. This technology should be developed further for finishing advanced ceramics. Investigation of mechano-chemical material removal methods would also be of great value to this field of research.

With these features in mind, the following topics are suggested for further research:

1. Using MAF technology for finishing advanced structural materials such as silicon nitride, PSZ, and alumina.

2. Mathematical investigation of magnetic flux behavior when using MAF for non-ferromagnetic materials, specifically studying the effect of magnetic pole shape on induced finishing pressures.

3. Synthesis and characterization of magnetic abrasive powders.

4. Development of mechano-chemical material removal methods for various advanced structural materials.

5. Optimization of process variables for maximum material removal rate and best finish.

6. Fundamental micromechanisms of material removal in MAF.

7. Characterization of the surface and near surface features on silicon nitride rods finished by MAF.

8. Correlation of strength and fatigue properties of silicon nitride rollers finished by MAF with processing conditions.

9. Comparison of strength, fatigue, and performing in service of components finished by MAF with those finished by conventional techniques.

10. Economics of MAF for application to the finishing of advanced ceramics.

11. Development of prototype MAF equipment for different applications.

Bibliography

Anzai, M., Kawashima, E., Otaki, H., and T. Nakagawa, "Magnetic Abrasive Finishing of WC-Co Curved Surfaces," *Machining of Advanced Materials,* Proceedings of the International Conference on Machining of Advanced Materials. Gathersberg MD, 20-22 July 1993,) NIST Special Publication No. 847, (1993), 415-422.

Baron, Y., M., "Magnetic Abrasive and Magnetic Machining of Machine Parts and Cutting Tools," Leningrad Machine Building, Leningrad, (1986).

Coats, H. P., "Method of and Apparatus for Polishing Containers," US Patent No. 2,196,058, dated April 2, (1940).

Evans, R. C., *An Introduction to Crystal Chemistry,* New York, New York: Cambridge University Press, (1964), 67-68.

McColm, I. J. *Ceramic Science for Materials Technologists.* New York, New York: Blackie & Son, (1983), 107-115.

Mekedonski, B. G., and A. D. Kotshemodov," Schleifen in Magnetfeld," Fertigungstechnik und Betrieb, 24, H.4, (1974), 230-235.

Shikhirev et al. , "Device for the Treatment of Sheet Materials," US Patent No. 4,040,209, (1980).

Shikhirev et al., "Apparatus for Treatment of Sheet Material with the use of Ferromagnetic Powder," US Patent No. 4,187,081, dated Feb. 5, (1980).

Shikhirev et al., "Apparatus for Working Sheet Materials with Ferromagnetic Powder," US Patent No. 4,204,370, dated May 27, (1980).

Shinmura, T., Hatano, E., and K. Takazawa, "The Development of Magnetic-abrasive Finishing and Its Equipment by Applying a Rotating Magnetic Field," *Bulletin of JSME*, Vol. 29, No. 258, 4437-4443, (1986).

Shinmura, T., Takaxawa, K., and E. Hatano, "Study on Magnetic Abrasive Finishing," *Bull. of Japan Soc. of Prec. Engg*, Vol. 21, No. 2, (1987), 139-141.

Shinmura, T., and T. Aizawa, "Study on Internal Finishing of a Non-Ferromagnetic Tubing by Magnetic Abrasive Machining Process," *Bull. Japan Soc. of Prec. Engg.*, Vol. 23, No. 1, (1988), 36-41.

Shinmura, T. and T. Aizawa, "Study on Magnetic Abrasive Finishing Process," *Bull. Japan Soc. of Prec. Engg.*, Vol. 23, No. 3, (1989), 236-239.

Simjian, L. G. (1956), "Sharpening or Polishing Device," US Patent No. 2,735,231, (1956).

Shinmura, T., "A Study on Mechanism of Magnetic Abrasive Polishing and Development of its Apparatus, " (1987).

Takazawa, K., Shinmura, and E. Hatano, " Development on Magnetic Abrasive Finishing and Its Equipment," MR 83-678. Proc. of the SME's 12th Deburring and Surface Conditioning Conference, Orlando, Nov. 8-10, (1983).

Vora, H., Orent, T. W., and R. J. Stokes, "Mechanochemical Polishing of Silicon Nitride," *Communications of the American Ceramic Society*, September 1982, C-140-C-141, (1982).

Washko, S. D., and G. Aggen, "Wrought Stainless Steels," *Metals Handbook*. 10th ed. Ohio: ASM International, V1, (1990), 841-907.

Appendix I: Magnetic Fields and Forces

Working on the magnetic field assisted finishing techniques requires some knowledge of magnetic field theory and the forces that are generated on material media. This appendix describes the topics which are of immediate concern to the engineer, but does not address the detailed physical issues which surrounds magnetic field theory.

The Magnetic Circuit

Perhaps the most intuitive approach to magnetic circuits is the analogy between electric and magnetic circuits. To make this analogy clear the following relationships are useful.

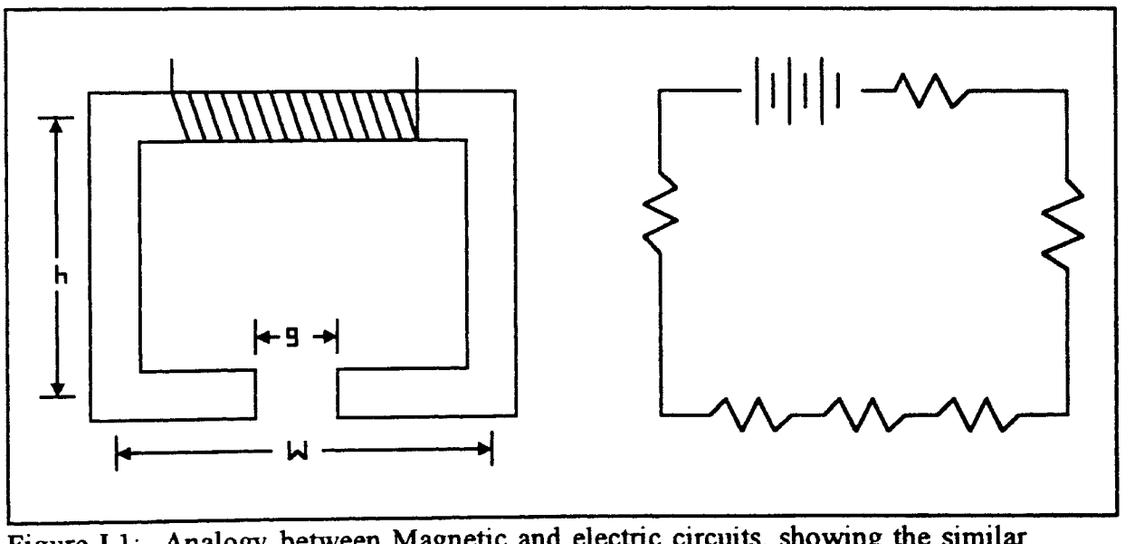

Figure I.1: Analogy between Magnetic and electric circuits, showing the similar components.

The magnetic circuit may be compared to an electric circuit if the electric circuit is thought of as lengths of wire with the resistance, r, of the wire in resistance per length (Ω/m or (V/A)/m). The EMF in this case must be given in EMF per length of wire (V/m). The equation for current flow, i (A), is then i=V/r. The same is true in the case of a magnetic circuit. Effort, is a result of current through a coil, is determined by K which has the units of "A turns". Dividing K by the magnetic path length gives the effort per length which is H and has the units of "A turns/m". Total magnetic flow, ϕ, is given in Weber (Wb) and the flux density, B, is flow/area or Wb/m^2 = 1 Tesla (T). Resistance of a magnetic circuit is a function of the magnetic permeability, μ, which is dependent on the magnetic flux carrying media. Permeability has the units of (A turns)/m/T.

Consider the two circuits in Figure I.1. The circuit on the left is a magnetic circuit, and the circuit on the right is the corresponding electrical circuit. The lengths of material that form the magnetic yoke each have a resistance to magnetic flux, thus corresponding to a resistor. The coil at the top of the magnetic yoke serves as the source of magnetic field, corresponding to the battery in the case of the electric circuit.

In the electric circuit the battery serves as a source of effort (voltage) which provides an effort for current flow. In the case of the magnetic circuit the coil provides the effort for magnetic flux. The amount of effort produced is the coil current density, K, which is given as

$$K=ni$$

where n is the number of turns in the coil and i is the current in the coil. The units of

K are A turns/m (meter is a result of definition). In the gaussian system of units K is given in Oe where 1 Oe = $1000/4\pi$ A turns/m (note that 1 Oe = 1 Gauss).

The resistance of elements in the circuit may be calculated by

$$R=\frac{l}{\mu A}$$

where l is the length of the element, μ is the permeability of the material, and A is the cross sectional area of the element. Resistances are added in series and parallel in the same way as electrical resistances are added.

Once K and R are known, ϕ in the air gap may be determined by

$$\phi=\frac{K}{R}.$$

When ϕ is determined, the field, H, in an area such as an air gap between poles may be determined by

$$H=\frac{\phi}{A\mu_0}$$

where A is the cross sectional area of the air gap.

Permeability of a material is not usually a constant, but is a function of H. Referenced values are usually given as the maximum permeability of the material. Figure I.2 is an example of how μ may vary with H. The graph starts at 0,0. The peak of the graph is μ_{max}. When μ reaches near zero values with high H, the material is said to be saturated. In the case of a vacuum, μ has a value of μ_0 which is $4\pi x10^{-7}$H/m. A term

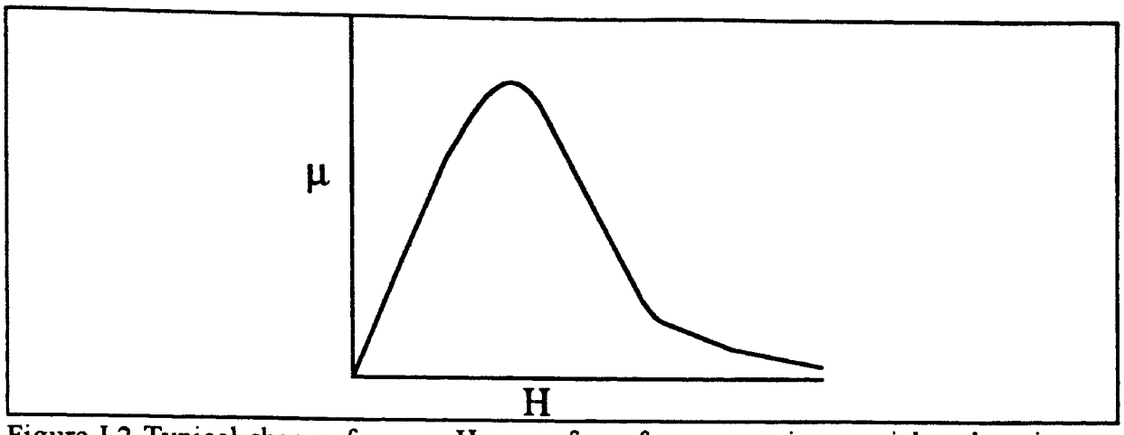

Figure I.2 Typical shape of a μ vs H curve for a ferromagnetic material such as iron.

Material	μ_r
Water	0.999991
Air	1.0000004
Cobalt	250
Mild Steel (0.2 C)	2000
Iron (0.2 impurity)	5000
78 Permalloy	100000
Purified Iron	200,000

Table I.1: Maximum permeability of selected materials.

commonly used is μ_r which is defined by μ/μ_0 for a material. Table I.1 lists some maximum μ_r values for some materials.

When measuring H, usually magnetic induction, B, is measured, then H may be determined by

$$B=\mu H$$

where μ is the permeability of the material. Since usually B is measured in air, H may be given as $H = B/\mu_0$. The units of B are Gauss (G) and Tesla (T) where $1G = 10^{-4}$ T.

Magnetic Forces

The force on an object with volume V and susceptibility X placed in a magnetic field is determined by

$$F=\mu_0 V\chi H\frac{dH}{dx}$$

in

the x direction. Susceptibility is given by

$$\mu=\mu_0(1+\chi) \quad \rightarrow \quad \chi=\mu_r-1$$

which indicates that X ~ μ_r for materials such as iron, cobalt, etc. which have relative permeability values much greater than 1. Note that just as μ is a function of H, X is also. A term which is convenient when working with forces is average magnetization given by

$$\overline{M}=\chi H$$

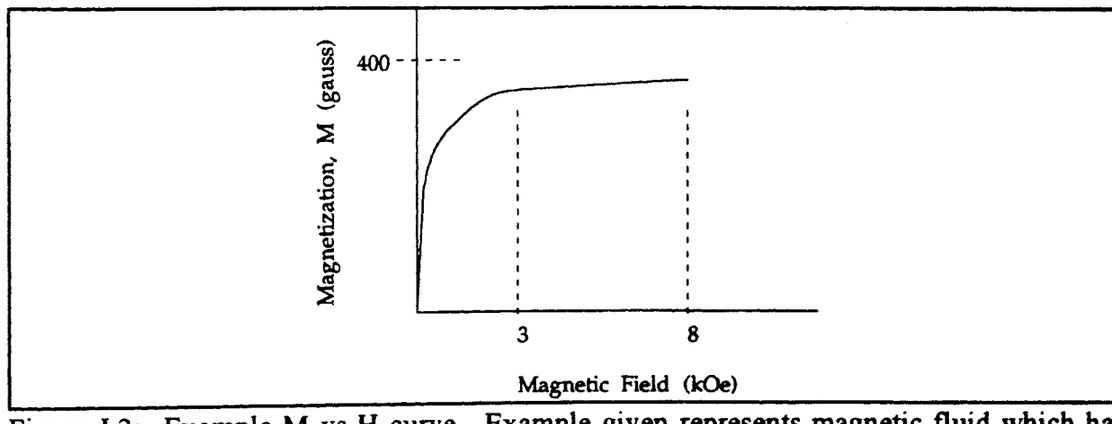

Figure I.3: Example M vs H curve. Example given represents magnetic fluid which has a saturation magnetization of 400 gauss.

which has the units of H, however sometimes M is multiplied by μ_0 to get units of B such as Gauss or Tesla. M is averaged over H to get average magnetization which is used to determine forces. It can be derived that in the linear region of magnetization, average M is 2/3 of the actual magnetization. Figure I.3 shows a typical relationship between M and H. The point in which dM/dH reaches near zero is the saturation point. If the M vs H relation is known for a material, forces may be calculated using

$$F=\mu_0 V\overline{M}\frac{dH}{dx}$$

which indicates that once the saturation value for M is reached, force increases linearly with the field gradient.

Appendix II: Schematic diagrams of built electronics

The following diagrams in Appendix II are schematics of the equipment built to control magnetic field strength etc. for the magnetic abrasive finishing apparatus. These components are interconnected by a DB25 connector, pins numbered DB1 through DB25.

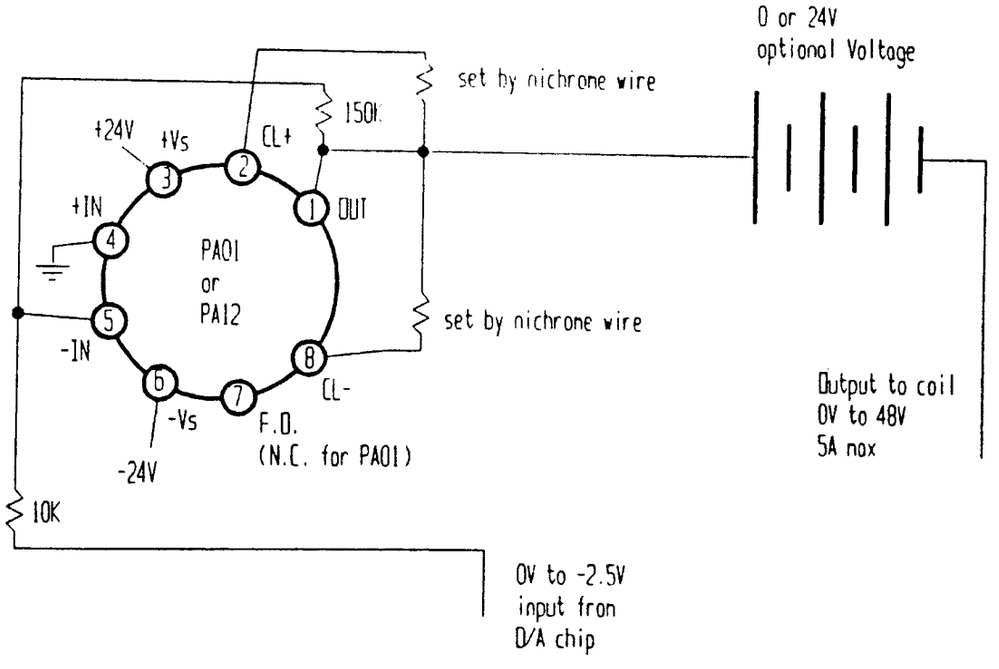

Figure II.1: Power amplifier and voltage supplies

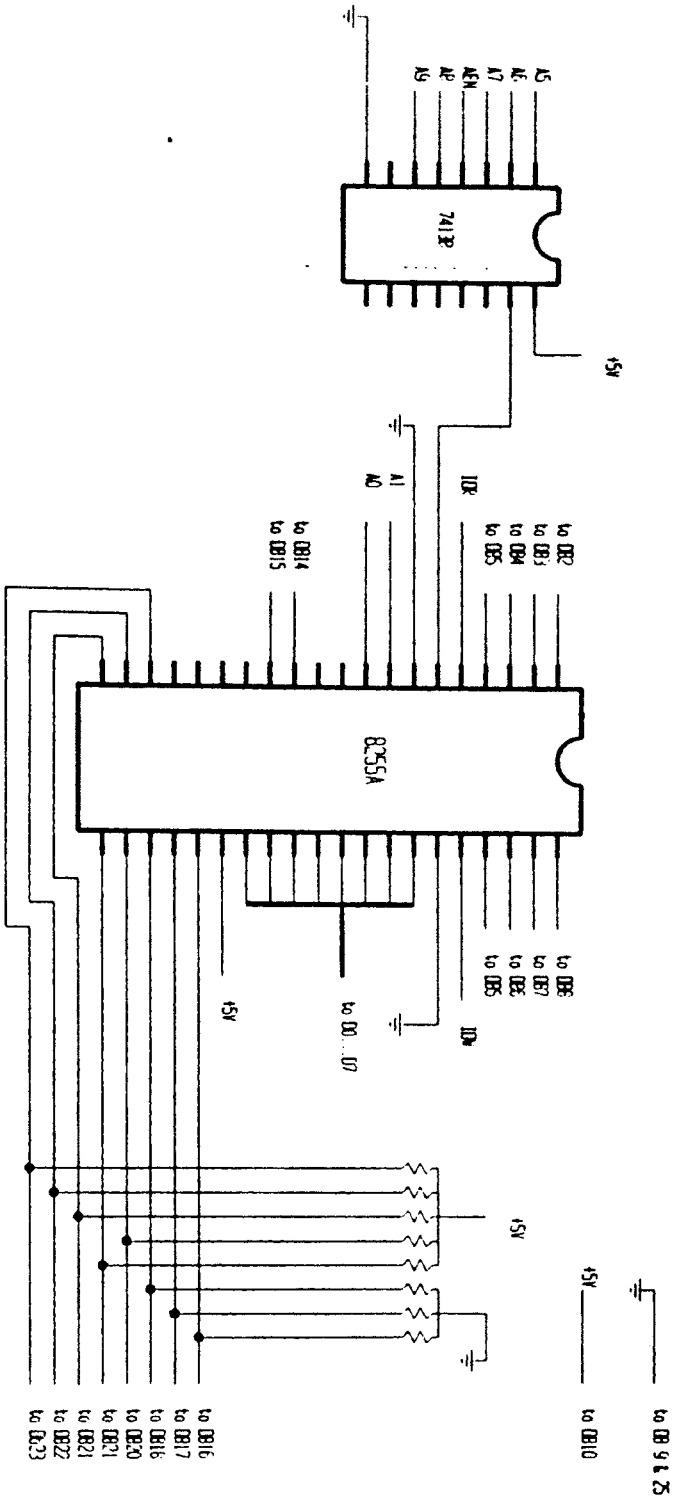

Figure II.2: 8255 I/O chip and supporting addressing chip

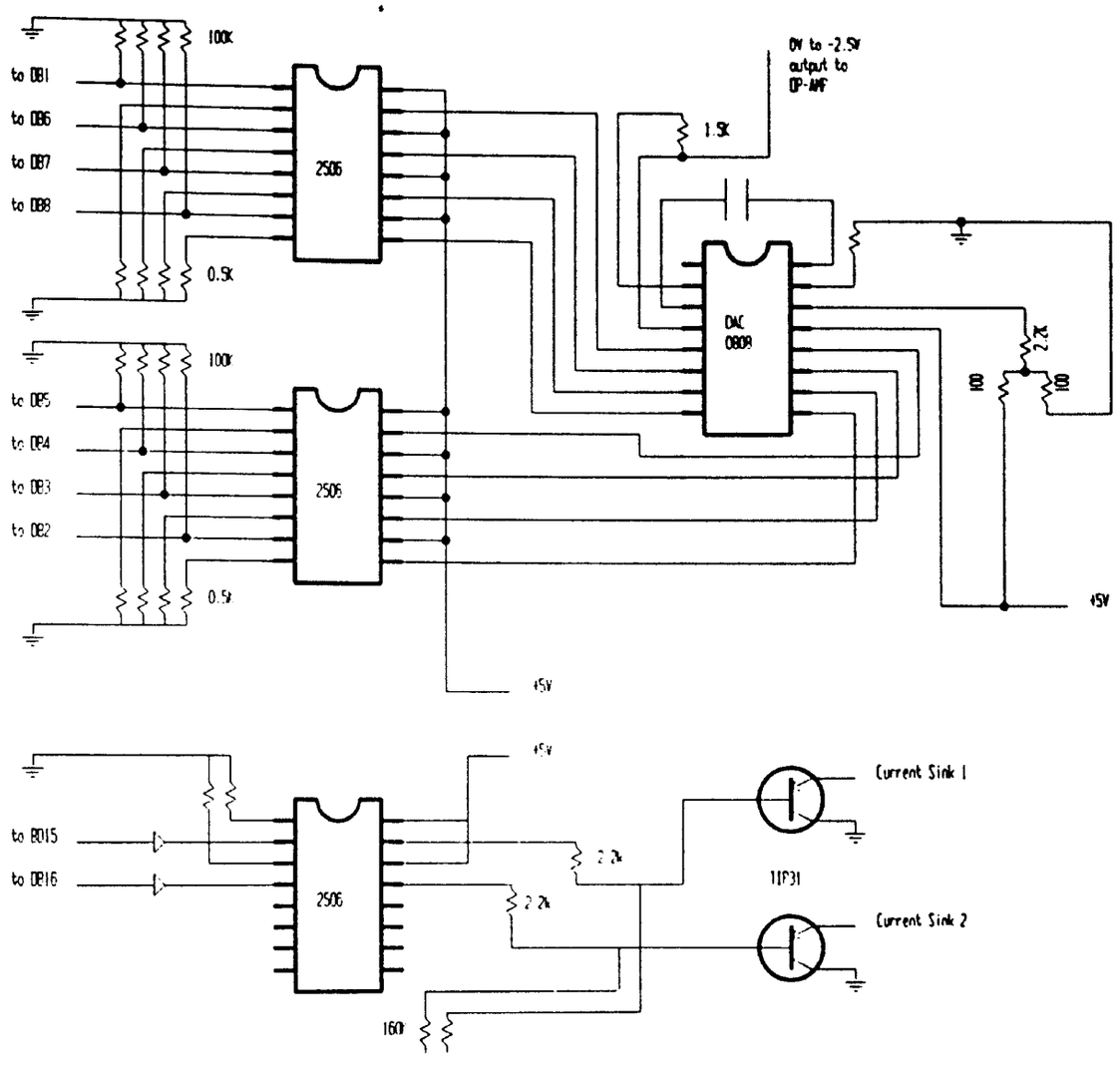

Figure II.3: Optical isolation circuits and D/A converter

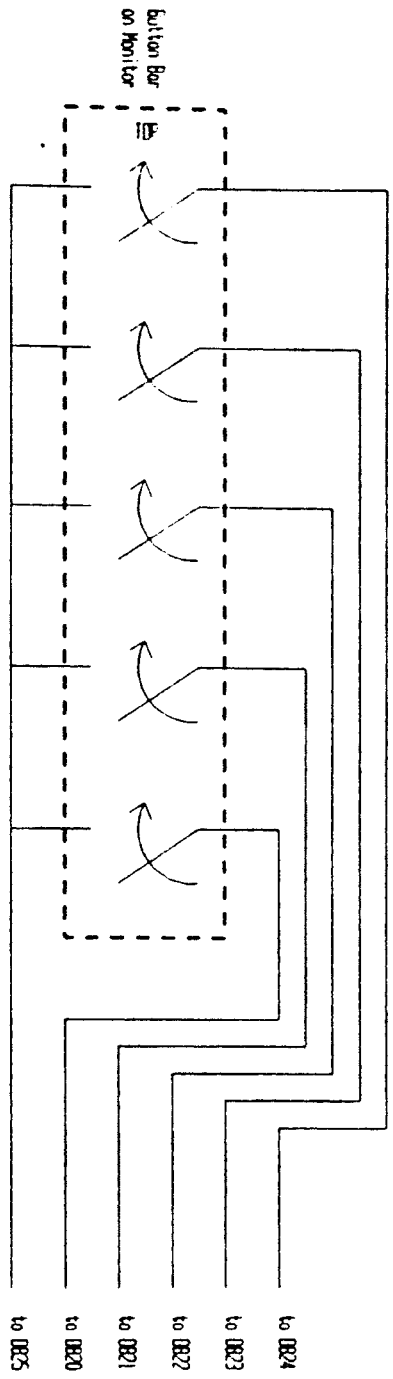

Figure II.4: Soft Keys

Appendix III: Source code for automatic control of MAF Equipment

This Appendix is the C source code used to control the magnetic abrasive finishing machine through the electronics shown in appendix II.

```
#include <stdio.h>
#include <stdlib.h>
#include <dos.h>
#include <time.h>
#include <conio.h>

#define DEBUG          1

#define PORT_FLD       0x200    // Port A
#define PORT_BUTTONS           0x201    // Port B
#define PORT_C                 0x202    // Port C
#define CTRL                   0x203    // Control register on 8255

#define POSITION       1       // Menu Idents
#define FIELD          2
#define TIME           3
#define CONTROL                4

#define POSINC                 1        // Position step size for each LED

#define STOP           0       // used for move
#define LEFT           1
#define RIGHT          2

#define RESET          2
#define ELAPSED                1
#define STOP           0
#define START          3

#define TRUE           1
#define FALSE          0

#define F1             49      //59
#define F2             50      //60
#define F3             51      //61
#define F4             52      //62
#define F5             53      //63
#define F6             54      //64

#define MAINMENU       1
#define FIELDMENU1     2
#define POSITIONMENU           3
```

```
#define TIMEMENU      4
#define CONTROLMENU         5
#define FIELDMENU2    6

#define PROCESS             1
#define OFF           2
#define ON            3
#define HOME            4

#define HEARTRATE     100
// ============================================================================
//                      Function Prototypes
// ============================================================================
void Heart();

void InitBoard();
int Position();
int CheckButtons();
int CurrentButtonsPressed();
int CurrentLED();

void Move(int);

void WriteMenu(int);

void DrawFrame();
void CommandTitle(char[10]);
void Command1(char[10]);
void Command2(char[10]);
void Command3(char[10]);
void Command4(char[10]);
void Command5(char[10]);
void Command6(char[10]);
void InitScreen();

void Automatic(int);

void ProcessMenu();

void Debug();

void FindZero();

void SetField(int);

double CalcTime(int);
void DisplayTime();
// ============================================================================
//                          Global Vars
// ============================================================================

int Home = 0,LLimit = 0,RLimit = 0;

// ============================================================================
```

```
//                      Main
// ============================================================================

void main()
{       //FindZero();
          InitBoard();
          InitScreen();
          CheckButtons();CheckButtons();
          WriteMenu(MAINMENU);
          CheckButtons();


          CalcTime(RESET);
          CalcTime(STOP);
          while(1)
          {
          if (DEBUG) Debug();
          DisplayTime();
          ProcessMenu();
          Automatic(PROCESS);
          Heart();
          }
}

void Debug()
{
static int LastBut, LastPos;
int CurrentBut, CurrentPos;
          CurrentBut = CurrentButtonsPressed();
          CurrentPos = Position();
          if ((CurrentPos != LastPos) | (CurrentBut != LastBut))
          {
          gotoxy(10,25);
          printf("%3i",CurrentBut);
          gotoxy(15,25); printf("%3i",CurrentPos);
          LastBut = CurrentBut;
          LastPos = CurrentPos;
          }
          return;
}

// ============================================================================
//                      sub: SetField
// ============================================================================

void SetField(int Magnitude)
{

          outportb(PORT_FLD,Magnitude);
          return;
}

// ============================================================================
//                      sub: FindZero
```

```
// ============================================================
void FindZero()
{
        clrscr();
        printf("Locating Machine Zero\n");
        printf("Allow automatic control");
        Move(RIGHT);
        while(CurrentLED()) Heart();
        Move(STOP);
        clrscr();
        printf("Found Zero");
        delay(3000);
        return;
}

// ============================================================
//                    sub: Automatic
// ============================================================

void Automatic(int Param)
{
static int AutoOn = 0,LastPos = 0,GoHome =0,CurrDir=STOP;
int CurrentPos;

        switch(Param)
        {
        case PROCESS:
          CurrentPos = Position();
 if (CurrentPos != LastPos)
 {
  gotoxy(22,5); printf("%3i",CurrentPos);
  LastPos = CurrentPos;
 }
 if (GoHome)
   {
    if (CurrentPos >= Home)
    {
    Move(STOP);
    GoHome = FALSE;
    }

   }
 if ((CurrentPos <= LLimit) & AutoOn &(CurrDir != RIGHT))
   {CurrDir = RIGHT;Move(RIGHT);}
 if ((CurrentPos >= RLimit) & AutoOn & (CurrDir != LEFT))
   {CurrDir = LEFT;Move(LEFT);}

 break;
case ON:
 AutoOn = TRUE;
 CalcTime(START);
 break;
case OFF:
 AutoOn = FALSE;
```

```
            CalcTime(STOP);
            break;
          case HOME:
            GoHome = TRUE;
            Move(RIGHT);
            CalcTime(STOP);
            break;
          }
          return;
}
// ============================================================
//                    sub: menu
// ============================================================

void ProcessMenu()
{
static int CurrentMenu = MAINMENU,FieldMag = 0,Fine=FALSE;
int Buttons;

          Buttons = CheckButtons();

          if (DEBUG && Buttons) {gotoxy(5,25);printf("%3i",Buttons);}

          switch(CurrentMenu)
          {
            case MAINMENU:
              if (Buttons & 1)
                { CurrentMenu = POSITIONMENU;
                  WriteMenu(POSITIONMENU);
                  break;
              }
            if (Buttons & 2)
              { CurrentMenu = FIELDMENU1;
                  WriteMenu(FIELDMENU1);
                  break;
              }
            if (Buttons & 4)
              { CurrentMenu = TIMEMENU;
                  WriteMenu(TIMEMENU);
                  break;
              }
            if (Buttons & 8)
              { CurrentMenu = CONTROLMENU;
                  WriteMenu(CONTROLMENU);
                  break;
              }
            if (Buttons & 16)
              { abort();
                  break;
              }
            else break;


          case FIELDMENU1:
```

```
case FIELDMENU2:
  if (Buttons & 16)
    { CurrentMenu = MAINMENU;
        WriteMenu(MAINMENU);
        break;
    }
  if (Buttons & 1)
    { FieldMag++;
        if (!Fine) FieldMag += 19;
        if (FieldMag > 255) FieldMag = 255;
        gotoxy(22,11);
        printf("%5.2f",(float)FieldMag/255*100);
        SetField(FieldMag);
        break;
    }
   if (Buttons & 2)
    { FieldMag--;
        if (!Fine) FieldMag -= 19;
        if (FieldMag < 0) FieldMag = 0;
        gotoxy(22,11);
        printf("%5.2f",(float)FieldMag/255*100);
        SetField(FieldMag);
        break;
    }
   if ((Buttons & 4)&&Fine)
    {
        Fine = FALSE;
        CurrentMenu = FIELDMENU1;
        WriteMenu(FIELDMENU1);
        break;
    }
  if ((Buttons & 4)&& !Fine)
    {
        Fine = TRUE;
        CurrentMenu = FIELDMENU2;
        WriteMenu(FIELDMENU2);
        break;
    }
  else break;

case POSITIONMENU:
  if (Buttons & 16)
    { CurrentMenu = MAINMENU;
        WriteMenu(MAINMENU);
        break;
    }
  if (Buttons & 1)
    { Home = Position();       // home
        gotoxy(22,9);
        printf("%3i",Home);
    }
  if (Buttons & 2)
    { LLimit = Position();
        gotoxy(22,7);
```

```
                printf("%3i",LLimit);
              }
            if (Buttons & 4)
              { RLimit = Position();
                gotoxy(22,8);
                printf("%3i",RLimit);
              }

            else break;

           case TIMEMENU:
            if (Buttons & 16)
              { CurrentMenu = MAINMENU;
                WriteMenu(MAINMENU);
                break;
              }
            else break;

           case CONTROLMENU:
            if (Buttons & 16)
              { CurrentMenu = MAINMENU;
                WriteMenu(MAINMENU);
                break;
              }
            if (Buttons & 1) Automatic(ON);
            if (Buttons & 2) {Automatic(OFF);Automatic(HOME);}
            if (Buttons & 8) {InitBoard();}
            break;
        }
return;

}

// ================================================================
//                  sub: time
// ================================================================

void DisplayTime()
{
static double last_time;
double current_time;
        current_time = CalcTime(ELAPSED);
        if (current_time != last_time)
        {
                gotoxy(23,16);
                printf("%i:%2i  ",(int)(current_time/60),
                        (int)(current_time-60*(int)(current_time/60)));
                last_time = current_time;
        }
        return;
}

double CalcTime(int instruction)
{
```

```
static time_t time1;
static double cumulative=0.0;
static int running=FALSE;
double time_diff=0.0;

        switch (instruction)
        {
                case RESET: time1 = time(NULL); cumulative = 0.0;
                            break;

                case START:
                        if(!running)
                        {
                        time1 = time(NULL);
                        running = TRUE;
                        }
                        break;

                case STOP :
                         if (running)
                           {
                            cumulative += difftime(time1,time(NULL));
                            running = FALSE;
                           }
                            break;

                case ELAPSED: time_diff = cumulative;
                              if(running)
                                   time_diff += difftime(time1,time(NULL));
                              break;


        }
        return(0.0-time_diff);
}

// ================================================================
//                  sub: move
// ================================================================
void Move(int Direction)
{
static int CurrentStat;
        outportb(PORT_C,(CurrentStat & 0xC0));
        switch (Direction)
        {
                case STOP: CurrentStat = (CurrentStat & 0xC0); break;          // 11000000
                case LEFT: CurrentStat = (CurrentStat | 0x30); break;          // 00110000
                case RIGHT:CurrentStat = ((CurrentStat & 0xC0) | 0x20); break;  // 00100000
        };

        delay(1000);
        outportb(PORT_C,CurrentStat);
        return;
}
```

```
// ============================================================
//                    Subs: Screen functions
// ============================================================

void WriteMenu(int WhichMenu)
{
        switch(WhichMenu)
        {
        case MAINMENU:
                CommandTitle("Main Menu");
                Command1("Position ");
                Command2("Field    ");
                Command3("Time     ");
                Command4("Control  ");
                Command5("Exit     ");
                break;
         case POSITIONMENU:
                CommandTitle("Position ");
                Command1("Home Pos ");
                Command2("L. Limit ");
                Command3("R. Limit ");
                Command4("         ");
                Command5("Main Menu");
                break;
          case TIMEMENU:
                CommandTitle("Time     ");
                Command1("Min Up   ");
                Command2("Min Down ");
                Command3("Sec Up   ");
                Command4("Sec Down ");
                Command5("Main Menu");
                break;
case FIELDMENU1:
                CommandTitle("Field    ");
                Command1("Mag Up   ");
                Command2("Mag Down ");
                Command3("Course   ");
                Command4("Mode     ");
                Command5("Main Menu");
                break;

 case FIELDMENU2:
                CommandTitle("Field    ");
                Command1("Mag Up   ");
                Command2("Mag Down ");
                Command3("Fine     ");
                Command4("Mode     ");
                Command5("Main Menu");
                break;

  case CONTROLMENU:
                CommandTitle("Control  ");
                Command1("Init Auto");
                Command2("Stop Auto");
```

```
                Command3("          ");
                Command4("Reset     ");
                Command5("Main Menu");
                break;
        }
        return;
}

// ================================================================
//                  Subs: DrawFrame and Commandx
// ================================================================
void DrawFrame()
{
int count = 0;
int line  = 0;

        clrscr();
        printf("   Automated Magnetic Field Assisted Finishing - Driver V1.0  M. Fox   OSU\n\n");

        printf("%c",213);

        while (count !=66)
        {
                printf("%c",205);
                count++;
        }
        count = 0;

        printf("%c",203);

        while (count != 11)
        {
                printf("%c",205);
                count++;
        }
        count = 0;

        printf("%c",187);

        while (line != 20)
        {
                printf("%c",179);

                gotoxy(wherex()+66,wherey());

                printf("%c",186);

                gotoxy(wherex()+11,wherey());

                printf("%c",186);

                line ++;
         }
         printf("%c",212);
```

```
        while (count !=66)
        {
                printf("%c",205);
                count++;
        }
        count = 0;

        printf("%c",202);

        while (count != 11)
        {
                printf("%c",205);
                count++;
        }
        count = 0;

        printf("%c",188);

        return;
}

void CommandTitle(char name[10])
{
        gotoxy(70,3);
        printf("%s",name);

        return;
}

void Command1(char name[10])
{
        gotoxy(70,6);
        printf("%s",name);

        return;
}
void Command2(char name[10])
{
        gotoxy(70,10);
        printf("%s",name);

        return;
}

void Command3(char name[10])
{
        gotoxy(70,14);
        printf("%s",name);

        return;
}

void Command4(char name[10])
{
```

```
        gotoxy(70,18);
        printf("%s",name);

        return;
}

void Command5(char name[10])
{
        gotoxy(70,22);
        printf("%s",name);

        return;
}

void Command6(char name[10])
{
        gotoxy(70,24);
        printf("%s",name);

        return;
}

// ================================================================
//                    sub: InitScreen
// ================================================================
void InitScreen()
{
        directvideo = 1;
        clrscr();
        DrawFrame();
        gotoxy(5,5); printf("Position      :");
        gotoxy(5,6); printf("Cycle Number  :");
        gotoxy(5,7); printf("L. Limit (in) :");
        gotoxy(5,8); printf("R. Limit (in) :");
        gotoxy(5,9); printf("Home     (in) :");
        gotoxy(5,11);printf("Field %       :");
        gotoxy(5,12);printf("Field    (T) :");
        gotoxy(5,13);printf("Current  (A) :");
        gotoxy(5,14);printf("Flied Mode    :");
        gotoxy(5,16);printf("Time     (m:s):");
        gotoxy(5,17);printf("Stop @   (s) :");
        gotoxy(5,18);printf("Interval (s) :");
        gotoxy(5,20);printf("Spindle  (RPM):");
        gotoxy(5,22);printf("Vibration     :");


        return;
}

// ================================================================
//                    sub: InitBoard
// ================================================================
void InitBoard()
{       clrscr();
```

```
        printf("Board Initialized");
        outportb(CTRL,130);
        delay(500);
        SetField(0);
        return;
}

// ============================================================
//                    sub: Heart
// ============================================================

void Heart()
{static int CurrentPos=0, count=0;

        count++;
        if (count == HEARTRATE)
        {
          count = 0;
          gotoxy(1,25);
          CurrentPos++;
          if (CurrentPos==8) CurrentPos = 0;
          switch (CurrentPos)
          {
            case 0: printf("/");break;
            case 1: printf("-");break;
            case 2: printf("\\");break;
            case 3: printf("|");break;
            case 4: printf("/");break;
            case 5: printf("-");break;
            case 6: printf("\\");break;
            case 7: printf("|");break;
          }
        }
        return;
}



// ============================================================
//                    sub: Position
// ============================================================
int Position()
{
static int LastLedPos = 0 ,CurrentPos = 0;
signed int CurrentLedPos, led, PositionInc;

        led = CurrentLED();
        switch(led)
        {
                case 192: CurrentLedPos = 1;  break;
                case 128: CurrentLedPos = 2;  break;
                case 160: CurrentLedPos = 3;  break;
                case 32 : CurrentLedPos = 4;  break;
```

```
                case 96 : CurrentLedPos = 5;  break;
                case 64 : CurrentLedPos = 6;  break;
                case 224: CurrentLedPos = 10; break;
                case 0  : CurrentLedPos = 10; break;

        }
        PositionInc= CurrentLedPos - LastLedPos;
        if (PositionInc < -4) PositionInc += 6;
        if (PositionInc > 4) PositionInc -= 6;
        LastLedPos = CurrentLedPos;
        CurrentPos += PositionInc*POSINC;

        return(CurrentPos);

}
// ============================================================
//                    sub: CheckButtons
// ============================================================

int CheckButtons()
{
static int LastButtons;
int Buttons, CurrentButtons,key;

        CurrentButtons = inportb(PORT_BUTTONS);
        CurrentButtons = (CurrentButtons ^ 0xFF); //  invert
        Buttons = (LastButtons ^ CurrentButtons); //  detect change
        Buttons = (Buttons & 0x1F);               // exclude high 3 bits
        Buttons = (Buttons & CurrentButtons);     // only pass if 1
        LastButtons = CurrentButtons;
        if (kbhit())
        {
                key = getch();
                switch(key)
                {

                case F1: Buttons = (Buttons | 1); break;
                case F2: Buttons = (Buttons | 2); break;
                case F3: Buttons = (Buttons | 4); break;
                case F4: Buttons = (Buttons | 8); break;
                case F5: Buttons = (Buttons | 16); break;
                case 113: abort();break;
                };


        }
        return(Buttons);
}
// ============================================================
//                    sub: CurrentButtonsPressed
// ============================================================

int CurrentButtonsPressed()
{
```

```
int Buttons;

        Buttons = inportb(PORT_BUTTONS);
        Buttons = (Buttons ^ 0xFF);
        Buttons = (Buttons& 0x1F);
        return(Buttons);
}
// ================================================================
//                    sub: CurrentLED
// ================================================================

int CurrentLED()
{
int led;

        led = inportb(PORT_BUTTONS);
        led = (led & 0xE0);
        return(led);


 }
```

VITA

Michael J. Fox

Candidate for the Degree of

Master of Science

Thesis: MAGNETIC ABRASIVE FINISHING OF NON-FERROMAGNETIC ROLLING ELEMENTS

Major Field: Mechanical Engineering

Biographical:

Personal Data: Born in Oklahoma City, Oklahoma, On Dec 18, 1969, the son of Larry and Charlene Fox.

Education: Graduated from Harrah High School, Harrah, Oklahoma in May 1988; Received Bachelor of Science degree in Mechanical Engineering with a minor in Mathematics from Oklahoma State University, Stillwater, Oklahoma in December, 1992. Completed the requirements for the Master of Science degree with a major in Mechanical Engineering at Oklahoma State University in December, 1994.

Experience: Employed by Oklahoma State University as an undergraduate teaching assistant for Dynamic System Modeling, Simulation and Design, and as a graduate teaching assistant for Metal Cutting. Undergraduate and Graduate research assistant under Dr. R. Komanduri in the field of advanced manufacturing processes.